Supplementary Information

Reductions in the deposition of sulfur and selenium to agricultural soils pose risk of future nutrient deficiencies

Aryeh Feinberg*, Andrea Stenke, Thomas Peter, Eve-Lyn S. Hinckley, Charles T. Driscoll, Lenny H. E. Winkel*

*Correspondence to: arifein@mit.edu (A.F.); lenny.winkel@eawag.ch (L.H.E.W.)

This PDF file includes:

Supplementary Discussion

Supplemental modelled deposition data

We show results for selenium (Se) and sulfur (S) deposition in past and future simulations in Supplementary Figures 1 and 2. Mapped source contributions for Se in past and future simulations are shown in Supplementary Figures 3–5. Supplementary Table 1 lists global emission fluxes of S and Se from different sources over the studied time periods. The mean, 10th percentile, and 90th percentile deposition over agricultural areas in the simulations is listed for S in Supplementary Table 2 and Se in Supplementary Table 3.

Impact of climate change on S and Se deposition

We ran a simulation with SSP5–8.5 S and Se emissions under recent climate conditions (2005–2009) to identify the impact of climate change on deposition under the more extreme Shared Socioeconomic Pathways (SSP) scenario. The relative difference between Se deposition under the SSP5–8.5 emissions and future climate and Se deposition under SSP5–8.5 emissions and recent climate is illustrated in Supplementary Figure 6a. The analogous S plot is shown in Supplementary Figure 6b.

Precipitation patterns are expected to change in the future climate. SOCOL-AER shows similar precipitation changes (Supplementary Figure 7) to other Coupled Model Intercomparison Project – Phase 5 (CMIP5) models[1]. Precipitation increases are projected in the eastern equatorial Pacific and the western Indian Ocean, which emerge as areas of increased deposition in the future (Supplementary Figure 1d). Selenium deposition is more sensitive than S deposition to changes in precipitation patterns with climate (Supplementary Figure 6), because wet deposition plays a more important role in atmospheric Se removal (80% of total deposition) compared to atmospheric S removal (70%).

Precipitation is predicted to increase over high-latitude regions in SOCOL-AER and other CMIP5 models[1], which contributes partially to the increase of S and Se deposition over the Southern and Arctic Oceans. Another climatic factor involved in S and Se cycling in the high latitudes is sea ice coverage, which decreases in the future due to climate warming. Emissions of dimethyl sulfide (DMS) and dimethyl selenide (DMSe) to the atmosphere are limited by the sea ice barrier[2–4]. Removal of sea ice enhances the release of volatile S and Se to the atmosphere, a feedback that has been observed for DMS in the Arctic over the past two decades[5]. Due to this feedback, our model projects an additional 0.5 Tg S and 0.25 Gg Se emissions in the Arctic and Southern Oceans. In our simulations, no transient behavior in the marine DMS and DMSe concentrations were assumed over the 21st century. The response of marine DMS levels to climate change has been investigated by other modelling groups, with feedbacks arising due to future changes in ocean acidification, marine temperatures, marine algae communities, and micronutrient availability[3,6,7]. However, there is no consensus on how marine DMS concentrations will evolve in the future[8,9], and no information about possible trends in DMSe concentrations. Our model also does not consider the temperature-dependent response of continental biosphere emissions of S and Se to climate change. The projected warming could enhance emissions of volatile species from the continental biosphere; for example, emissions of isoprene are predicted to increase by 22–55% by 2100[9,10]. Excluding these additional feedbacks

that were not included in our model, the impacts of climate change on S and Se deposition are mainly limited to marine areas, especially in polar regions.

European deposition observations

Selenium wet deposition fluxes were measured at five German European Monitoring and Evaluation Programme (EMEP) sites (https://projects.nilu.no//ccc/reports.html) for 2006–2007 and 2015–2016, with no data available in between the two periods: Langenbrügge (52.8° N, 10.8° E), Schauinsland (47.9° N, 7.9° E), Neuglobsow (53.2° N, 13.0° E), Schmücke (50.7° N, 10.8° E), Westerland (54.9° N, 8.3° E). Westerland reported no measurement for 2006, so only the year 2007 data were collected for that site. In Supplementary Figure 8, we compare the modelled and observed changes in Se wet deposition between the earlier and later period. For each location, we average the model over the same years that were available from the observations. Additionally, bulk Se deposition data are available from Plynlimon, UK between 1999 and 2011[11,12]. For comparison with the German EMEP sites, we compare modelled and observed changes in bulk Se deposition between the period 1999–2000 and 2010–2011 (Supplementary Figure 8). SOCOL-AER captures the decadal changes in deposition from these European measurement stations (modeled = –37 ± 10% per decade, observed = –47 ± 18% per decade).

Analysis of SO_2 emissions in SSP scenarios

We focused on two future socioeconomic scenarios in this study, SSP1–2.6 and SSP5–8.5. To investigate whether the conclusions we make for 2100 apply to other scenarios, we plotted regional sulfur dioxide (SO_2) emissions in the seven other available scenarios from Gidden et al.[13] in Supplementary Figure 9. For this analysis, we focus on the other Tier 1 scenarios (SSP2-4.5 and SSP3–7.0). The SSP2–4.5 scenario, a middle-of-road scenario, shows similar 21st century anthropogenic SO_2 decreases as SSP1–2.6 even though the transition from fossil fuels to renewable energy is delayed[13]. SSP3–7.0, the regional rivalry scenario, shows the smallest global decreases in SO_2 emissions because of continuing coal combustion and low pollution control technology implementation in developing countries. In SSP3–7.0, anthropogenic emissions increase in Africa (+57% between 2015 and 2100) and South America (+31%), whereas Asian SO_2 emissions decreases are moderate (–25%) compared to SSP5–8.5 (–82%) and SSP1–2.6 (–96%). Nevertheless, SO_2 emission decreases are similar between SSP3–7.0 and SSP5–8.5 in North America (–40 to –50%) and Europe (–60%). Therefore, if we assume that anthropogenic Se-to-S emissions scaling holds similarly as it has in the past[14], the main outcome presented for SSP1–2.6 and SSP5–8.5 can be generalized for other future scenarios: S and Se inputs from the atmosphere will become scarcer by the end of the 21st century in North America, Europe, and Asia.

Comparison of Se emissions with national emission inventories

In order to produce estimates of anthropogenic Se emissions, we scale anthropogenic SO_2 emissions using the median scaling factor derived from a top-down analysis[14]. We compare the scaled Se emission estimates and the derived Se-to-S emission ratio with available data from national bottom-up emission inventories. This comparison elucidates whether the scaling approach yields reasonable results compared to bottom-up data, in order to confirm if it can be used to produce future projections of Se emissions.

China

China is one of the major emission sources of S and Se, accounting for approximately one third of global anthropogenic emissions for the period 2005–2009. Tian et al.[15] produced a comprehensive inventory of Se emissions for China, accounting for sources such as coal combustion, non-coal combustion, metal smelting, manufacturing of non-metallic products (i.e., glass, cement, and brick), biomass burning, and waste incineration. The inventory is calculated using annual source activities from China Statistical Yearbooks and time-varying emission factors that depend on the emission process, province, and the installed air pollutant control technology. The Chinese emission inventory for 1949–2012 is compared to our emission estimates in Supplementary Figure 10. Our approach of scaling SO_2 emissions using a time-invariant scaling factor is compatible with the bottom-up inventory. The Chinese emission trend over time matches between the two approaches. Tian et al.[15] computed the uncertainty of the total national Se emissions for 2010, considering the uncertainties in source activities and emission factors. Our scaled estimate is within the 95% confidence interval of the bottom-up study for 2010, showing that the two approaches are consistent.

USA

The USA Environmental Protection Agency (EPA) provides a comprehensive inventory of air pollutant emissions, including SO_2 and Se, in the National Emissions Inventory (NEI), available from https://www.epa.gov/air-emissions-inventories/national-emissions-inventory-nei. Emissions data from point, nonpoint, on-road, and non-road sources are compiled mainly using estimated emission factors and reported source activities, although for a minority of point sources, emission estimates are calculated using stack measurements. Total Se emissions for 2008 are lower in the NEI (0.29 Gg Se yr^{-1}) than our estimated USA emissions using the SO_2 scaling approach (0.81 Gg Se yr^{-1}). However, this discrepancy could be related to missing point sources for Se in the inventory or incorrect Se emission factors. There are substantially (~ 10 ×) more SO_2 point sources than Se point sources reported in the NEI, suggesting that it is plausible that not all Se sources are tracked.

Since there is a possible under-reporting of Se point sources, we analyze the subset of emission processes for which both SO_2 and Se data are reported in the NEI. A single polluting facility can have multiple *emission processes*, defined as an activity that leads to emissions. These emission processes are categorized by Source Classification Codes (SCCs) by the EPA, which can be used to classify emission processes in broader source categories. We compare the mean Se-to-S emission ratios in these point sources to our inverse modelling estimate based on measurements of Se in aerosols[14]. Supplementary Figure 11 displays the Se-to-S emission ratios for the major Se sources in the NEI dataset for 2008–2017. The NEI is compiled every three years, hence there are four datasets available in this timespan.

The major Se sources in the USA during this time period are coal combustion for energy generation, glass manufacturing, non-ferrous metal smelting, and cement manufacturing. The Se-to-S emissions ratio of different source categories varies by orders of magnitudes in the NEI database (Supplementary Figure 11). Glass manufacturing generally shows the highest ratio of Se-to-S emissions. Selenium is used to decolorize glass, because the pink tint of selenium compounds counterbalances the green and yellow colors caused by trace iron in the glass[16].

During the glass manufacturing process, Se is volatilized and emitted to the atmosphere. Coal combustion, currently the primary source of Se emissions in the USA, has a median Se-to-S emission ratios of approximately 10^{-4}, although this varies between ~10^{-6} and ~10^{-3} depending on the emission process (Supplementary Figure 11).

We calculate the mean Se-to-S ratio in the NEI by dividing the total Se emissions by total SO_2 emissions, with total emissions summed over only the emission processes that report both SO_2 and Se data. For 2008–2017, the mean NEI Se-to-S ratio ranges between 0.7×10^{-4} and 1.7×10^{-4} g Se (g S)$^{-1}$. These values agree well with the median inverse estimate for North America from Feinberg et al.[14], 1.8×10^{-4} g Se (g S)$^{-1}$. Therefore, the Se-to-S scaling approach used in this study is consistent with the mean values from the NEI data. Given the diversity of source Se-to-S emission ratios in the NEI, it is clear that our use of a spatially and temporally constant anthropogenic Se-to-S emission ratio is an approximation of reality. However, this approximation yields good agreement between our model and available Se observations[14], and it adequately represents the mean Se-to-S ratio in the bottom-up EPA inventory. In the future, further analysis of bottom-up emission inventories and high-resolution modeling studies would be necessary to further characterize how Se-to-S emission ratios vary over time and space.

Canada

Canadian anthropogenic emissions of SO_2 and Se are compiled in the National Pollutant Release Inventory (NPRI) from Environment and Climate Change Canada, available from https://www.canada.ca/en/services/environment/pollution-waste-management/national-pollutant-release-inventory.html. The inverse estimate for the anthropogenic Se-to-S emission ratio[14] is compared with the mean estimate from sources in the NPRI where both Se and SO_2 emissions were reported in Supplementary Figure 12a. Canadian Se emissions reported in the NPRI, categorized by source type, are displayed in Supplementary Figure 12b. Before 2011, very few point sources reported Se emissions, and therefore total Se emissions are very small and the overall Se-to-S emission ratios are not representative. After 2011, the NPRI estimate for the mean Se-to-S emissions ratio is relatively constant and lower than the inverse estimate used in this study by a factor of 3.

The seeming bias between our scaling approach and the bottom-up NPRI inventory is surprising, given the success of our simulations in matching Canadian aerosol Se measurements[14]. Our simulations showed a mean normalized bias of +16% compared to Canadian measurements, and the model was within a factor of 2 of measurements at 94% of sites. This comparison points to a possible low bias in the NPRI inventory for Se emissions. When Se emissions in the NPRI are separated by source categories, almost all of the anthropogenic Se emissions are from metal refining sources (Supplementary Figure 12b). Electricity sources of Se, including coal combustion for energy generation, are negligible in the NPRI, which is unrealistic given the importance of this source in the EPA inventory. We suspect that the NPRI may be missing Se emissions from coal combustion, biasing the mean Se-to-S emission ratio in Supplementary Figure 12a. We found examples of several major Canadian coal combustion power plants, and major sources of SO_2, which do not list Se emissions, e.g., Sundance Power Station in Duffield, AB; Keephills Generating Station in Duffield, AB; Sheerness Generating Station in Hanna, AB; and Belledune Generating Station in Belledune, NB. Facilities responsible for 38% of Canadian

SO_2 emissions in 2016 do not report any Se emissions, illustrating a possible under-reporting issue of Se emissions in the NPRI.

UK

Emissions of SO_2 and Se from the UK are reported in the National Atmospheric Emissions Inventory (NAEI), available at https://naei.beis.gov.uk. The emission inventory spans a period of 1970–2018, although the quality of Se emission estimates likely improved over time. An earlier report from the NAEI asserted that the quality of the Se emission inventory was low and that several emission factors were not representative[17]. The most recent report from the NAEI states that Se is among the heavy metals associated with the lowest uncertainties in the emission inventory[18]. Supplementary Figure 13a shows the trend in Se-to-S emission ratios over time in the UK and Supplementary Figure 13b shows the trends in Se emissions, both separated by source category.

The inverse estimate for the Se-to-S emission ratio, which we use in this study, is generally higher than the total Se-to-S emission ratio from the NAEI inventory (Supplementary Figure 13a). The NAEI inventory shows an increasing trend over time in the anthropogenic Se-to-S emission ratios. However, it is not clear if this pattern is related to the actual trends or refinements in the emission factor estimates over time. In more recent years, the UK emissions in the NAEI are closer to the emissions used in SOCOL-AER but are still 43% lower in 2017 (Supplementary Figure 13b). The comparison between our model and non-urban aerosol Se measurements in the UK between 1970 and 2013 showed a small mean normalized bias (–15%) and 78% of model values within a factor of 2 of measurement sites[14]. Thus, SOCOL-AER is slightly low-biased compared to the aerosol measurements, despite including higher UK emissions than in the NAEI.

Conclusions for comparisons with bottom-up inventories

Our approach for calculating SO_2 emissions yields consistent results with the Chinese Se emission inventory[15] and the American NEI. The comparison between the scaling approach and the Canadian and UK emission inventories is more ambiguous, due to possible issues with the Se emission data in these bottom-up inventories. Given the currently available atmospheric Se observations[14] and bottom-up inventories, the approach of scaling SO_2 emissions to calculate Se emissions is reasonable. However, further atmospheric monitoring and refinement of Se emission factors will be essential to determining whether this scaling approach holds for future emission projections, since the source composition of Se will continue to evolve and further pollution control technologies will be applied to point sources.

USGS stream data

Trends in all studied basins

We selected 18 stations from the USGS database that had an appropriate sampling frequency (more than 6 samples per year for Se) over a period of more than 9 years (Supplementary Table 4). These sampled watersheds are spread across the United States (Supplementary Figure 14), covering a range of hydrological, land cover, biogeochemical, and anthropogenic conditions. As opposed to Fig. 4 in the paper, in Supplementary Figure 15 we plot modelled deposition and measured stream fluxes of Se in absolute flux units, to illustrate changes to the surface Se mass

balance. Stream fluxes of sulfate, nitrate, and orthophosphate are plotted in relative units, so that changes in these nutrients can be compared to dissolved Se fluxes.

Certain similarities in the watershed behavior are evident in different geographic regions of the USA. Sites 1–4 are all located in the Eastern USA and deposition fluxes of Se are similar in magnitude or greater than dissolved stream fluxes of Se (Supplementary Figure 15). This pattern implies that atmospheric deposition is a major source of Se to these watersheds, and it would be more likely to observe an effect of the decreasing deposition trend on stream fluxes. Indeed, in all four of these sites the Se stream fluxes decrease after 2010, following decreases in deposition trends. Measurements from site 3 on the Ohio River shows that the watershed has changed from being a net sink of Se from the atmosphere to being a net source of Se. Stream fluxes of sulfate also shows a decline at sites 1–4, which would be compatible with decreasing S deposition in these watersheds. Several previous studies have attributed decreasing stream sulfate fluxes in Eastern USA watersheds to trends in atmospheric S deposition[19–22]. Rice et al.[19] found that different watersheds show different lags between S deposition decreases and stream sulfate decreases, due to differing retention processes in the catchment. The Ohio River watershed shows an ~8 yr lag between the decline in Se deposition and the decline in stream Se fluxes, which may represent the lag until legacy Se is flushed from the catchment. Since other sites in Eastern USA have only begun measuring Se stream concentrations in 2008, it is unclear whether these sites also show a lag period. In sites 1–4, the stream sulfate and Se fluxes show distinct trends from the nitrate and orthophosphate trends. Nitrate and orthophosphate are considered markers of urban wastewater and agricultural pollution[23]. The differing trends between sulfate/Se and nitrate/orthophosphate would be compatible with the hypothesis that declining S and Se deposition drives the decline in sulfate and Se stream fluxes, rather than declining agricultural or wastewater sources.

For the sites 5–12 in the Midwestern USA, stream fluxes of Se are generally larger than atmospheric deposition fluxes (Supplementary Figure 15). The relatively smaller deposition fluxes suggest a more limited influence on stream flux trends in these watersheds, compared to the Eastern USA sites. In sites 5–7, stream fluxes of Se decrease between 2008 and 2019. In the Yazoo River Basin, the decreases in sulfate and Se stream fluxes contrast with increasing nitrate and orthophosphate trends, which could be explained by the decreasing S and Se deposition inputs. However, it remains a possibility that other sources of S and Se have declined in this region, or that sulfate and Se have different retention mechanisms than nitrate and orthophosphate in this watershed. In the Wabash River and White River Basins, all four stream parameters decline over time. It is therefore difficult to conclude how the atmospheric deposition declines contribute to Se stream trends for these watersheds, since declining wastewater and/or agricultural inputs to the watershed could also explain trends in Se stream fluxes trends. Sites 8–12 are located in the Mississippi-Missouri river system and thus cover overlapping watersheds. These watersheds include a high proportion of cropland areas (Fig. 4). Stream Se fluxes tend to show increasing or stable trends over the measured period for these watersheds. In these basins, sulfate, nitrate, and orthophosphate fluxes generally show increasing trends (except for orthophosphate in site 11). The increases in these nutrients imply increasing agricultural inputs to these watersheds, which would also result in increasing Se inputs because Se is a trace constituent of phosphate fertilizers and animal manure[24]. The rising sulfate fluxes in the

Mississippi-Missouri river watersheds could be caused by increasing S application in USA agricultural fields[22].

Sites 13–16 in Colorado are characterized by the highest dissolved Se fluxes reported across the USA. Since the dissolved Se fluxes are much larger than our modelled Se deposition fluxes in these basins, trends in deposition likely have minimal effect on the watershed Se mass balance. Sites 13–15 all show decreasing trends in Se since the year 2000, while site 16 shows an increasing trend since the year 2000. These catchments could be affected by geogenic sources of Se. Much of the Rocky Mountain area was covered by an inland sea during the Late Cretaceous period (100–66 Ma), leading to shale deposits that are particularly enriched in Se [25–27]. Irrigation of agricultural areas mobilizes Se from rocks and soils in the area, which combined with high evaporation fluxes leads to elevated aquatic concentrations of Se and in certain cases toxic conditions for wildlife[27,28]. The observed trends in Se could result from changes in irrigation flows within the watersheds, although changes to urban point sources in these watersheds should also be further investigated[27].

The San Joaquin (site 17) watershed is particularly well-known for high Se levels, which have caused toxic conditions for wildlife in the past. The basin is an important agricultural area in the USA, but because of the arid conditions, farmlands are extensively irrigated[29]. Due to the presence of seleniferous bedrock in the region, the groundwater that is used for irrigation contains high concentrations of Se[24,30]. In the 1980s, the toxic Se concentrations in the watershed caused the Kesterson Reservoir disaster, during which birds and fish developed deformities[24]. This disaster resulted in a number of remediation projects in the region, including an effort to reuse saline and high Se irrigation water for growing plants that tolerate those conditions[29,31]. This project also limits the return of irrigation drainage water to the San Joaquin River, which could explain the concurrent decreases of stream Se, sulfate, and nitrate (Supplementary Figure 15). Orthophosphate does not show as strong of a decreasing trend as the other nutrients, perhaps due to P being the limiting nutrient in the catchment[32]. This basin has also been affected by prolonged droughts, e.g., an extended period between 2011–2015[29], which would affect nutrient fluxes. However, the flow-normalization in Weighted Regressions on Time Discharge and Season (WRTDS) aims to remove the influence of hydrological variability on the plotted fluxes and thus makes it easier to extract the long-term Se trend independent of annual discharge anomalies[33].

Powder River Basin (site 18) is another interesting case study of a watershed that may be affected by a particular Se source. The region is characterized by coal mining activities, which can release Se and sulfate in the mine drainage water[34,35]. Powder River Basin supplies around 40% of the total USA coal production, containing some of the largest coal mines in the USA. However, due to the declining use of coal generated energy in the USA, coal production in the Powder River Basin has declined by 35% from its peak in 2008 to 2018[36]. Reduced mining activities may be contributing to the decreasing trend in stream fluxes of Se and sulfate.

Concentration-discharge relationships

Another analysis tool that has been used in hydrology to characterize the sources and biogeochemical behaviour of chemical compounds are concentration-discharge (CQ) relationships[33,37–39]. Decreasing slopes of concentration vs. discharge plots, e.g., for Se at

Susquehanna River in 2008 (Supplementary Figure 16), are suggestive of dilution (source-limited) behaviour, where increasing discharges dilute the concentration. Flat slopes, e.g., for Se at Susquehanna River in 2019 (Supplementary Figure 16), indicate chemostatic behaviour and are associated with a homogeneous distribution of the compound throughout the catchment or stability of flow paths in the watershed with respect to discharge. Increasing slopes, e.g., for orthophosphate in Susquehanna River (Supplementary Figure 16), are indicative of transport-limited behaviour, in which enhanced discharges lead to mobilization of the compound or increased transport from an area where the compound is abundant[38,39]. The CQ relationship depends on the chemical properties of a compound (e.g., solubility and reactivity), and the hydrological (e.g., flow patterns) and biogeochemical (e.g., microbial activities, sorption/retention) properties of a watershed[39]. We present trends in CQ relationships of Se, nitrate, sulfate, and orthophosphate by month for six example watersheds (Supplementary Figures 16–21). This analysis can be conducted on WRTDS models using code available at: https://owi.usgs.gov/blog/plotFlowConc/.

In the CQ relationships of the three sites in Northeastern USA, the Se and sulfate plots show a similar pattern (Supplementary Figures 16–18). In 2008, all Northeastern sites show a downward-sloping or dilution behaviour for Se and sulfate. Over time, the concentration of Se and sulfate decreases throughout the discharge range. These concentration changes would be compatible with a diminishing background input of atmospheric deposition of Se and sulfate to the watershed. For certain months and sites, e.g., Se in August at the Susquehanna River site (Supplementary Figure 16), the concentrations at lower discharges decrease more strongly over time than the concentrations at higher discharges, leading to a flatter CQ relationship by 2019. Analysis of the CQ relationships of different compounds can provide further indications of whether the compounds share the same source in the different watersheds. Nitrate and orthophosphate generally show upward-sloping or transport-limited behaviour in the Susquehanna River (Supplementary Figure 16) and Ohio River (Supplementary Figure 18) sites. It is therefore plausible that nitrate and orthophosphate originate from sources that are not homogeneously distributed throughout the catchment, such as agricultural fields or storm water drainage. Additionally, at all three sites the concentration trends of nitrate and orthophosphate differ from that of Se and sulfate. The CQ relationships add further evidence that different sources and/or biogeochemical processes govern sulfate and Se in these watersheds, compared to the agricultural nutrients nitrate and orthophosphate.

In the Mississippi River (Supplementary Figure 19) and Platte River (Supplementary Figure 20) Basins, all nutrients generally show positive temporal trends in concentrations for most values of stream discharge. In the San Joaquin River Basin (Supplementary Figure 21), Se, sulfate, and nitrate show negative temporal trends for concentrations, whereas for orthophosphate the trend in concentration depends on the season. As opposed to the sites in Northeastern USA, Se and sulfate do not always show dilution behaviour in the CQ plots for the Platte and San Joaquin Basins (Supplementary Figures 20 and 21). For example, a local maximum in Se and sulfate concentrations occurs for higher discharges during the summer months. In the Platte River Basin, nitrate and phosphate generally show upward sloping CQ relationships, although without a local maximum at the same discharges as Se and sulfate (Supplementary Figure 20). Even if Se and sulfate have similar agricultural sources to nitrate and orthophosphate, differing biogeochemical processes (e.g., biological transformation, retention) within the watershed could lead to separate

CQ relationships between Se/sulfate and nitrate and orthophosphate[39]. In the San Joaquin Basin, the CQ relationships for nitrate and phosphate display a similar pattern to Se and sulfate, with maximum concentrations for intermediate levels of discharge (Supplementary Figure 21). Sulfate and Se may be mobilized from a similar source region as nitrate and phosphate (e.g., agricultural fields), which is only connected to the San Joaquin River above intermediate levels of discharge. By 2019, the Se concentration in the San Joaquin has decreased substantially from its 2008 levels, so that the local maximum in concentration is no longer observed. The efforts to prevent return of irrigation drainage water to the San Joaquin River appears to have changed the CQ behaviour of Se within the watershed to a source-limited relationship.

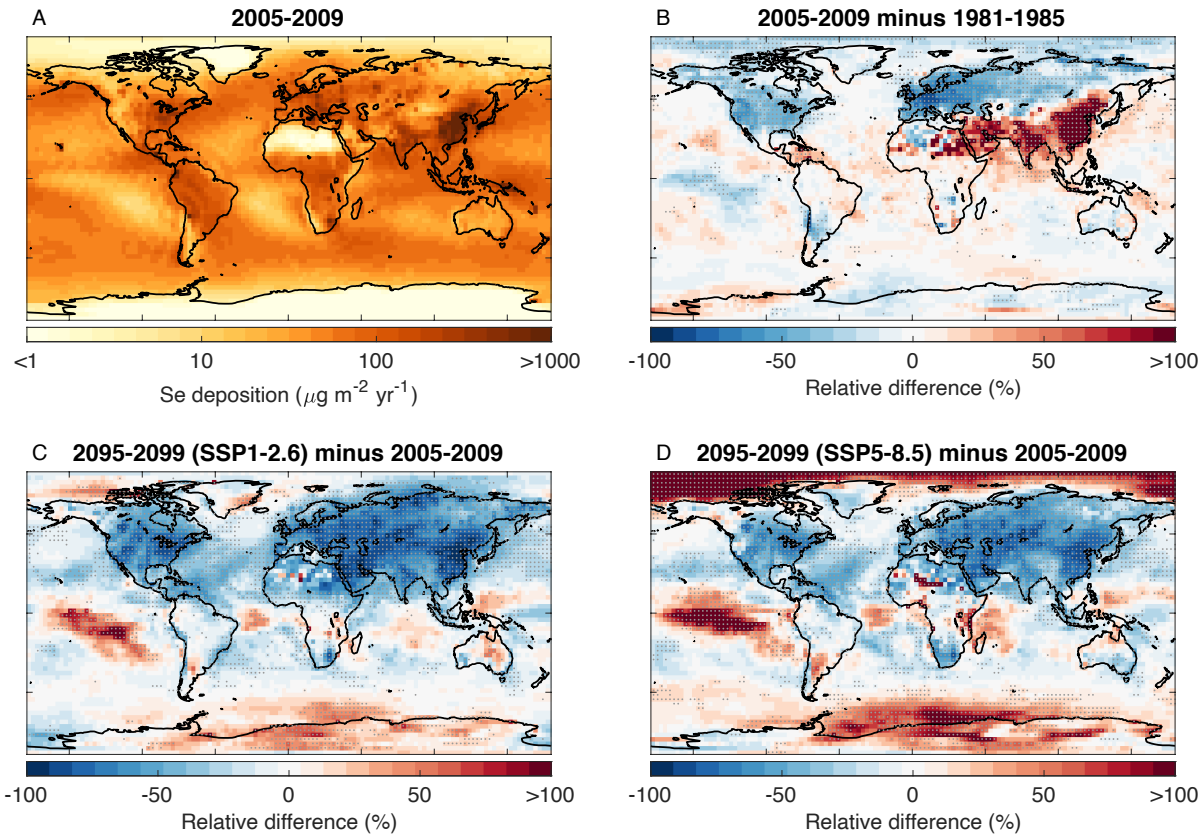

Supplementary Figure 1. Mapping Se deposition for the past and future. (a) Distribution of atmospheric Se deposition in the recent period, 2005–2009. Differences with the recent period are shown **(b)** for 1981–1985, **(c)** for 2095–2099 under the SSP1–2.6 scenario, and **(d)** for 2095–2099 under the SSP5–8.5 scenario. Stippling indicates grid cells where the mean change is larger than the 2σ interannual variability from the 2005–2009 simulation.

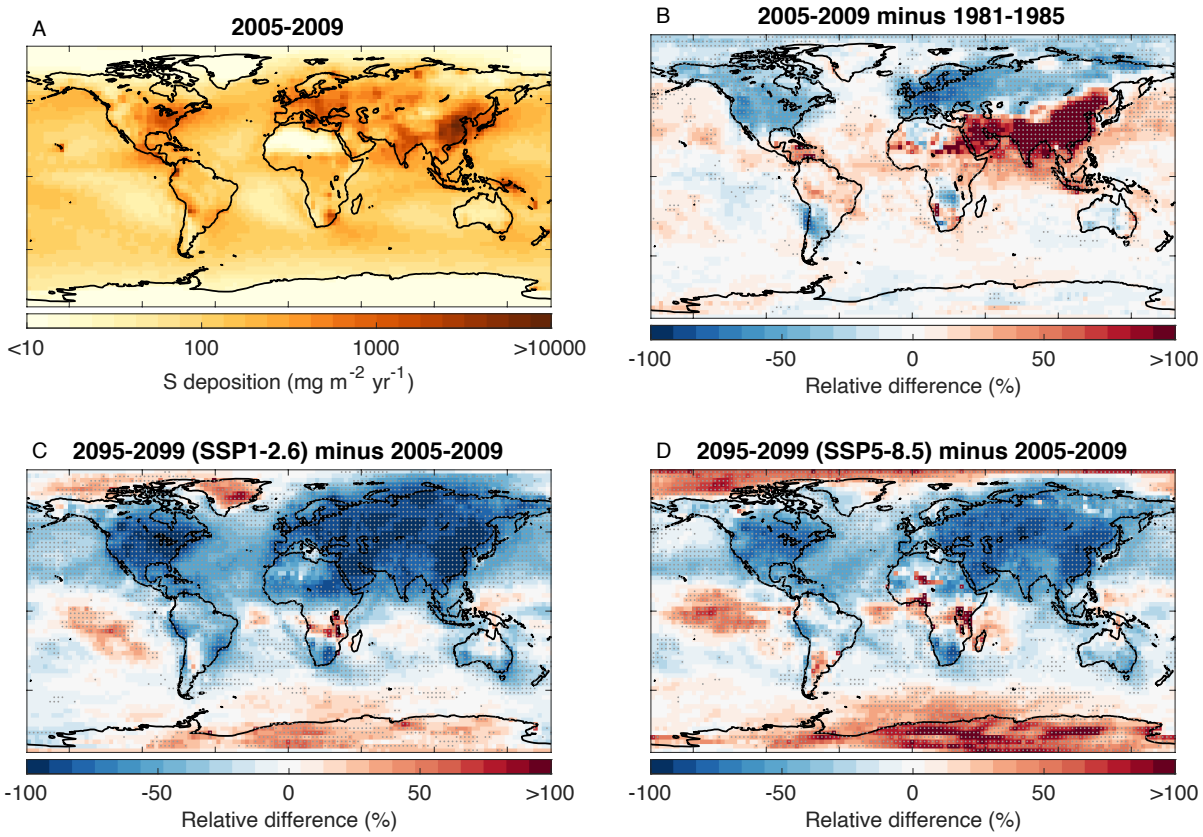

Supplementary Figure 2. Mapping S deposition for the past and future. (a) Distribution of atmospheric S deposition in the recent period, 2005–2009. Differences from the recent period are shown **(b)** for 1981–1985, **(c)** for 2095–2099 under the SSP1–2.6 scenario, and **(d)** for 2095–2099 under the SSP5–8.5 scenario. Stippling indicates grid cells where the mean change is larger than the 2σ interannual variability from the 2005–2009 simulation.

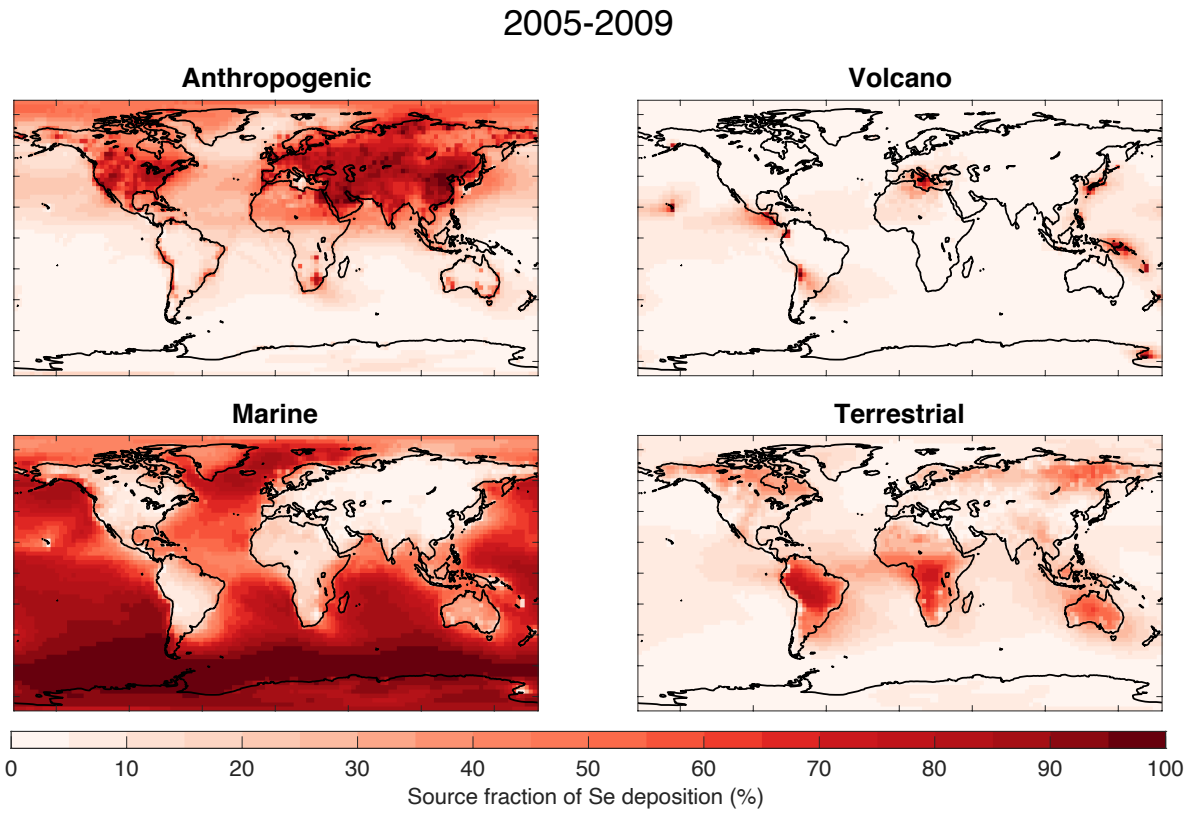

Supplementary Figure 3. Source contributions to Se deposition for 2005–2009.

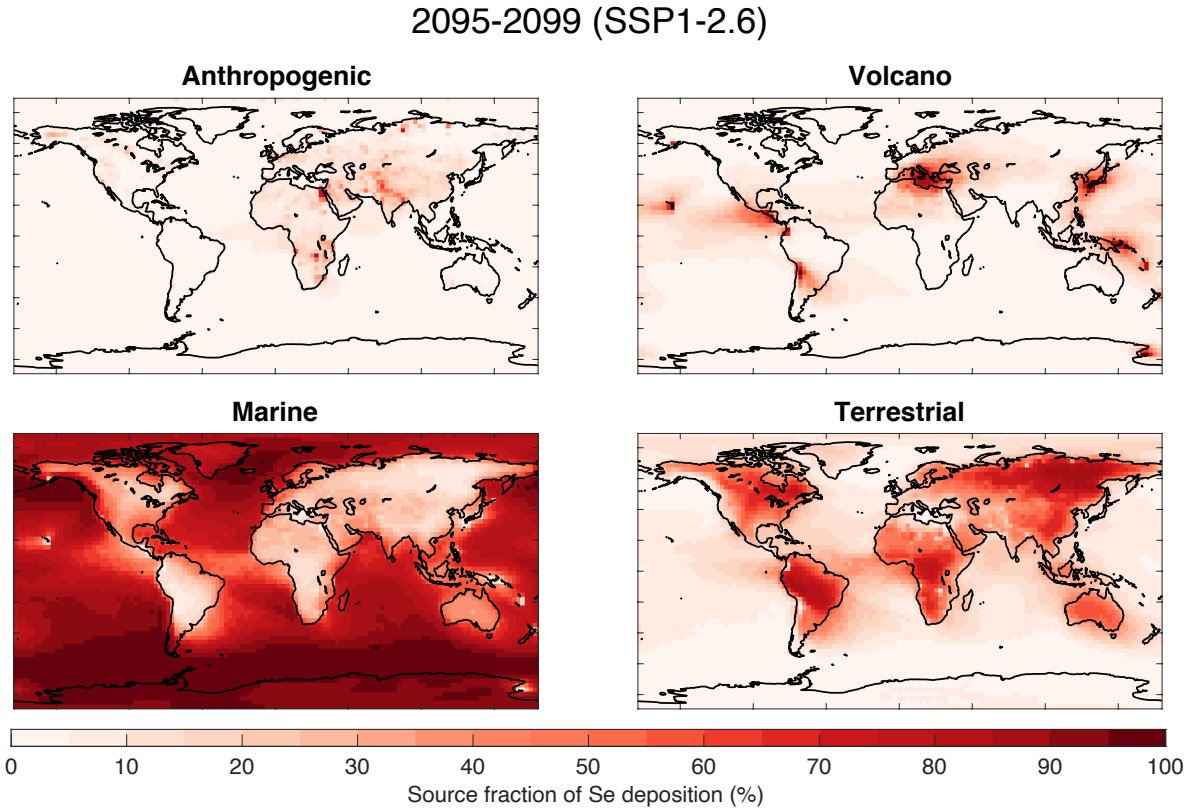

Supplementary Figure 4. Source contributions to Se deposition for SSP1–2.6 scenario, 2095–2099.

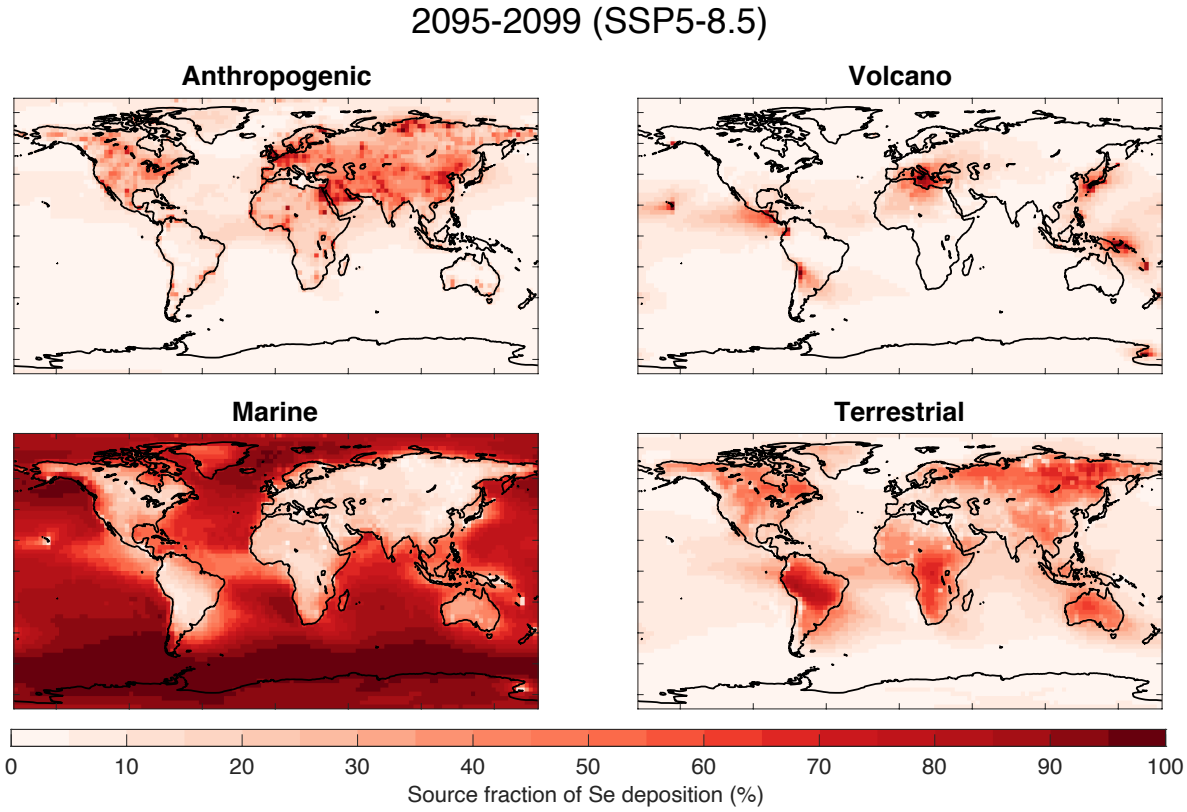

Supplementary Figure 5. Source contributions to Se deposition for SSP5–8.5 scenario, 2095–2099.

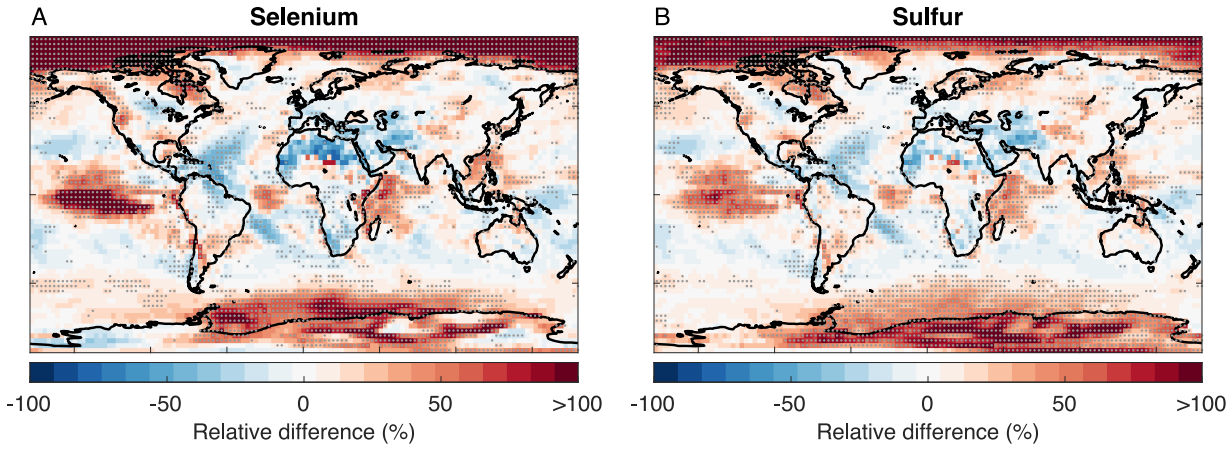

Supplementary Figure 6. Impact of climate change on (a) selenium and (b) sulfur deposition in the SSP5–8.5 scenario. Two simulations are compared: Simulation 1 with SSP5–8.5 emissions and climate and Simulation 2 with anthropogenic emissions of S and Se from SSP5–8.5 but using 2005–2009 values for climate forcing (i.e., sea-surface temperatures, sea-ice coverage, and greenhouse gas concentrations). The relative difference is shown, subtracting deposition in Simulation 2 from Simulation 1, i.e., red areas have higher deposition under SSP5–8.5 climate conditions than under 2005–2009 climate conditions. Stippling indicates grid cells where the mean change is larger than the 2σ interannual variability from the simulation with 2005–2009 climate conditions.

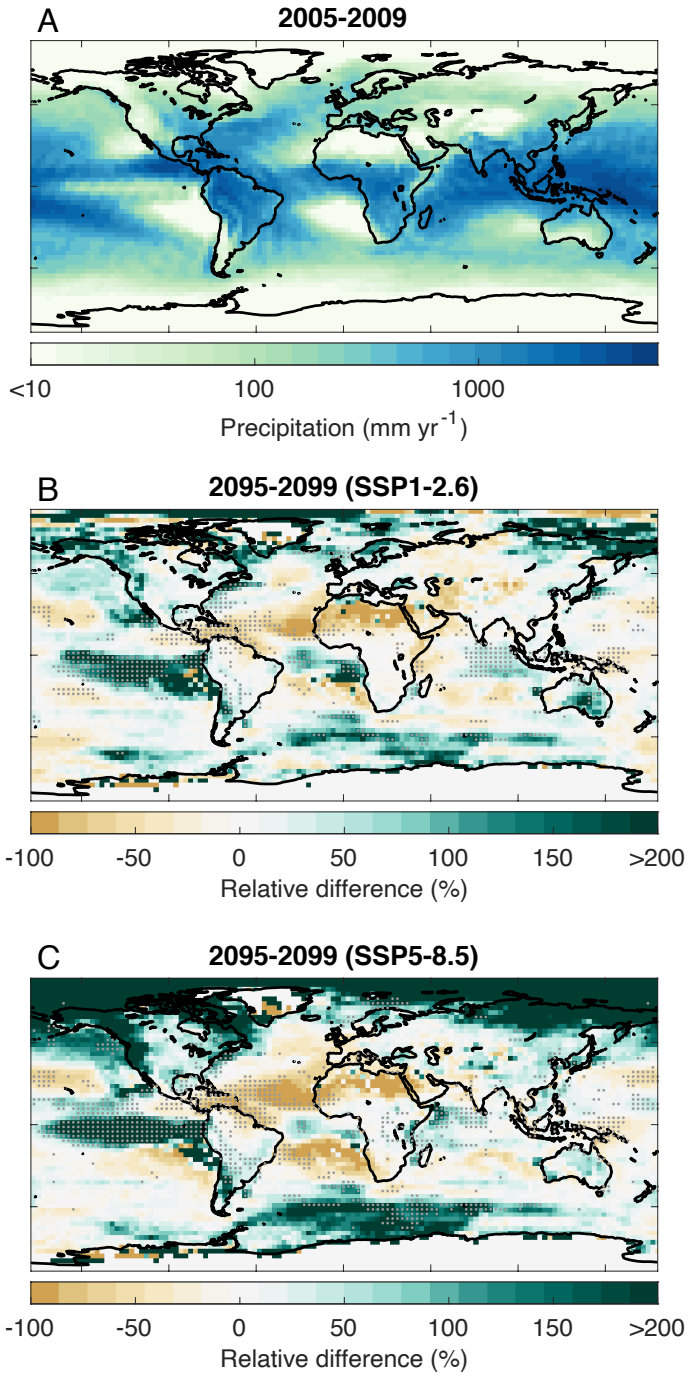

Supplementary Figure 7. Impact of climate change on precipitation in SOCOL-AER. (a) The distribution of simulated precipitation in the recent period, 2005–2009. Differences from the recent period are shown **(b)** for 2095–2099 under the SSP1–2.6 scenario, and **(c)** for 2095–2099 under the SSP5–8.5 scenario. Stippling indicates grid cells where the mean change is larger than the 2σ interannual variability from the simulation with 2005–2009 climate conditions.

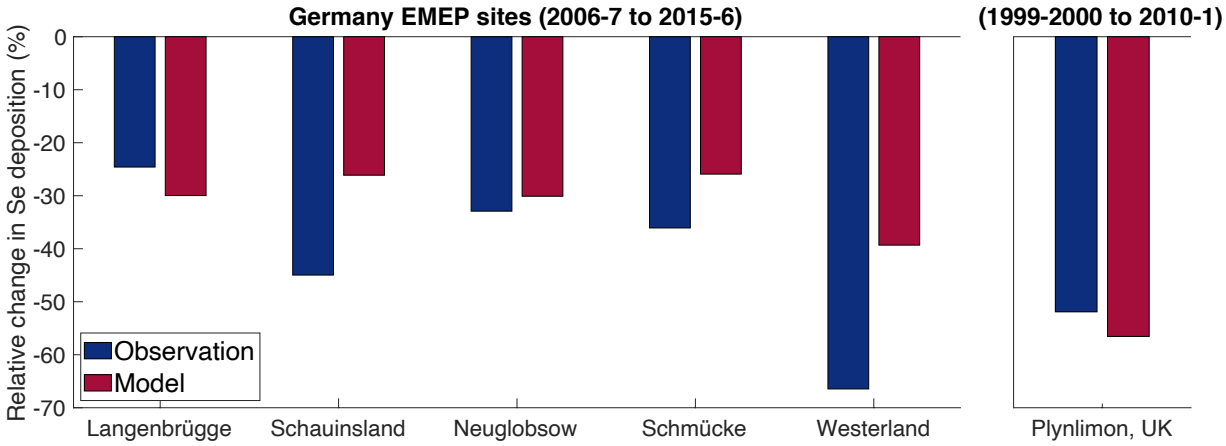

Supplementary Figure 8. Modelled and observed decadal changes in wet Se deposition from German EMEP sites and bulk Se deposition at Plynlimon, UK.

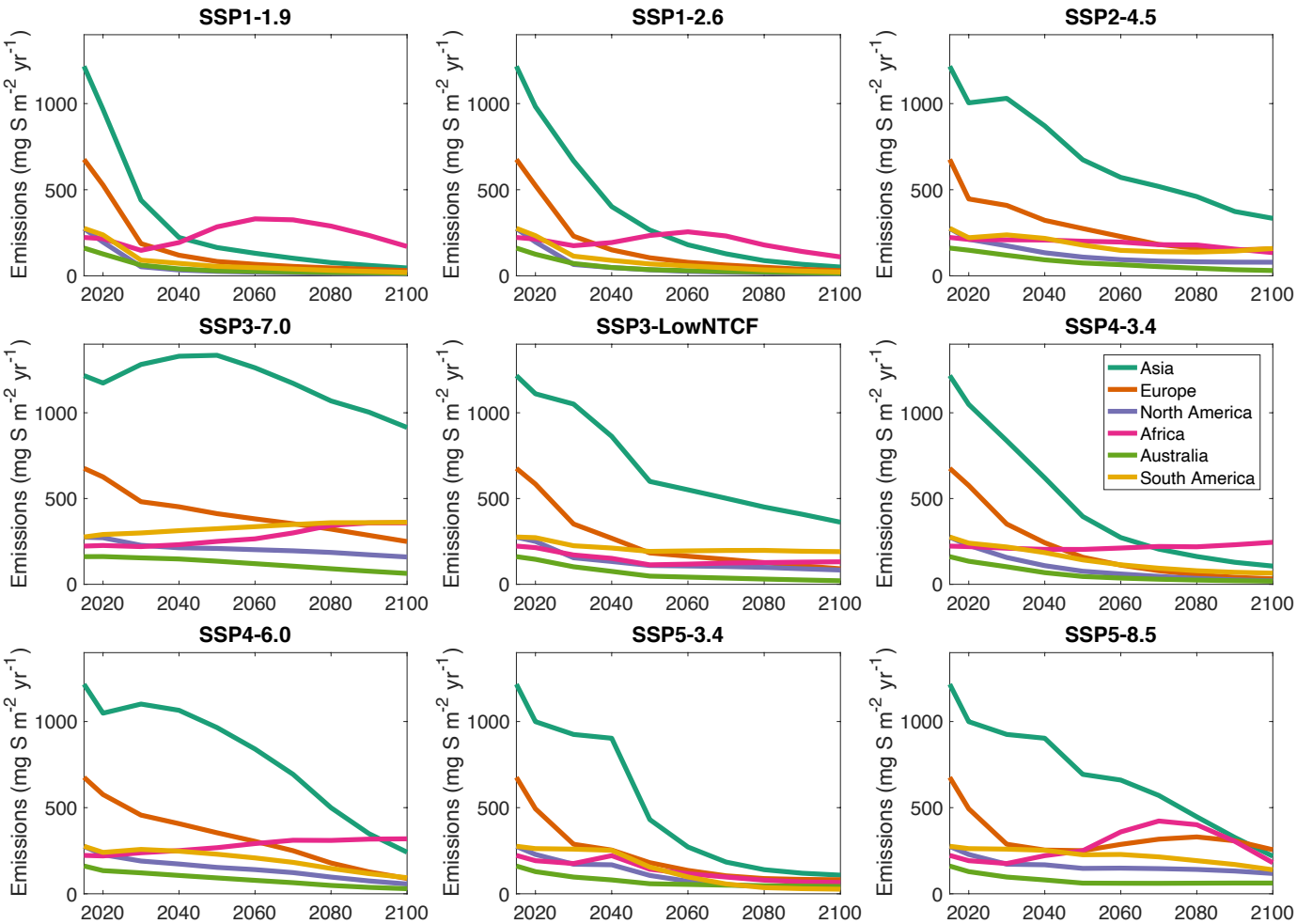

Supplementary Figure 9. Projected regional SO_2 emission trends from Gidden et al.[13], under different socioeconomic scenarios.

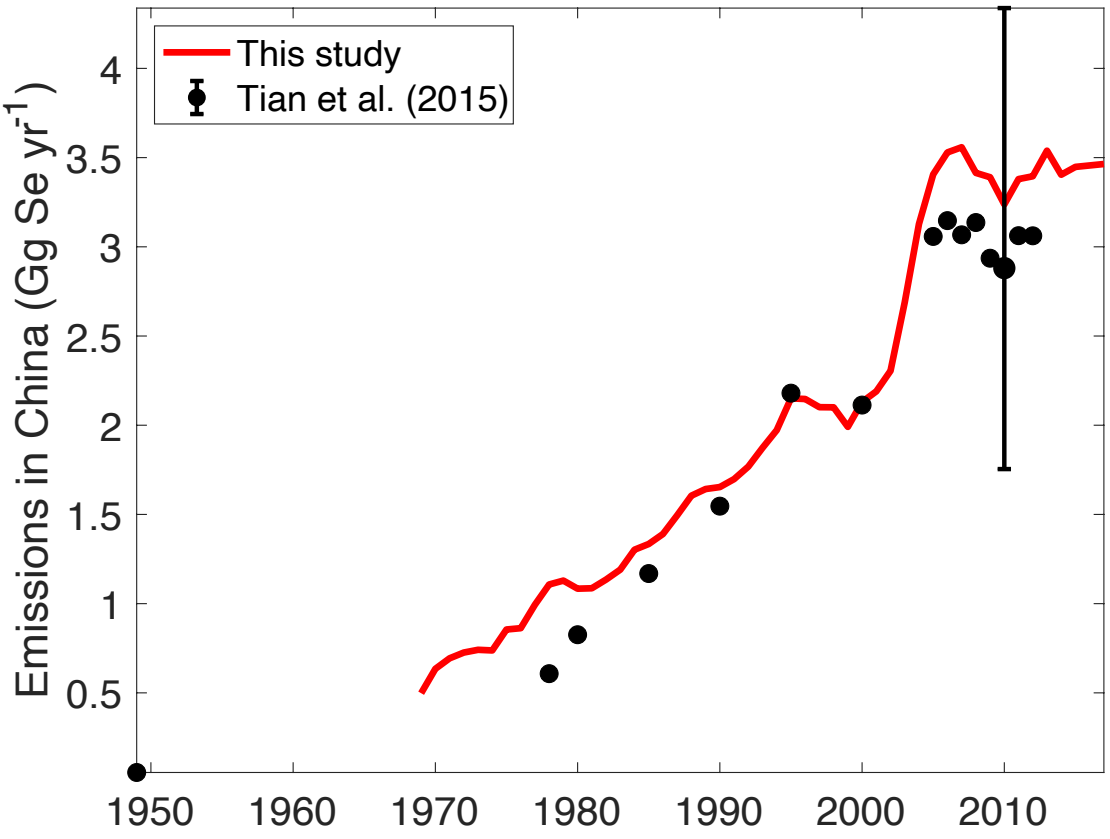

Supplementary Figure 10. Comparison between anthropogenic Chinese emissions of Se used in this study with bottom-up estimates from Tian et al.[15]. The error bar shows the 95% confidence interval of the Tian et al.[15] inventory for 2010.

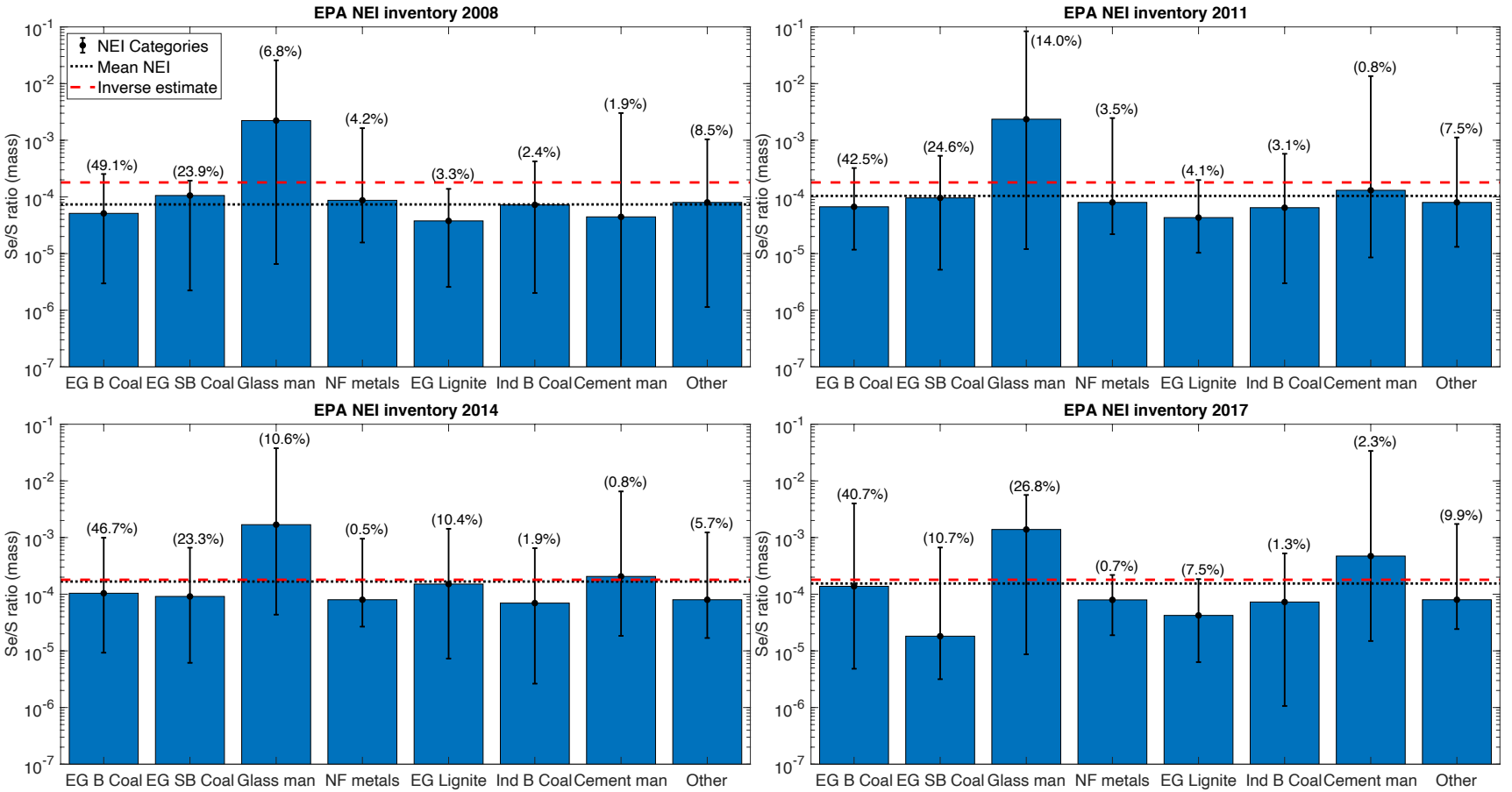

Supplementary Figure 11. Se-to-S emission ratios in the EPA NEI inventory for 2008–2017. All emission processes are categorized based on their EPA Source Classification Code. Source categories are abbreviated with the following: energy generation (EG), bituminous (B), sub-bituminous (SB), manufacturing (man), non-ferrous (NF), and industry (Ind). Median, 10th, and 90th percentile values of the Se-to-S emission ratio are shown for the major Se source categories of the NEI from these years. The percentages in parentheses on the plot indicate the fraction of total emissions for each source category. The dotted black line shows the mean Se-to-S emission ratio over all emission processes where both Se and S are reported in the NEI. This can be compared to the dashed red line, which shows the Se-to-S emission ratio derived from an inverse modelling study of aerosol Se observations[14].

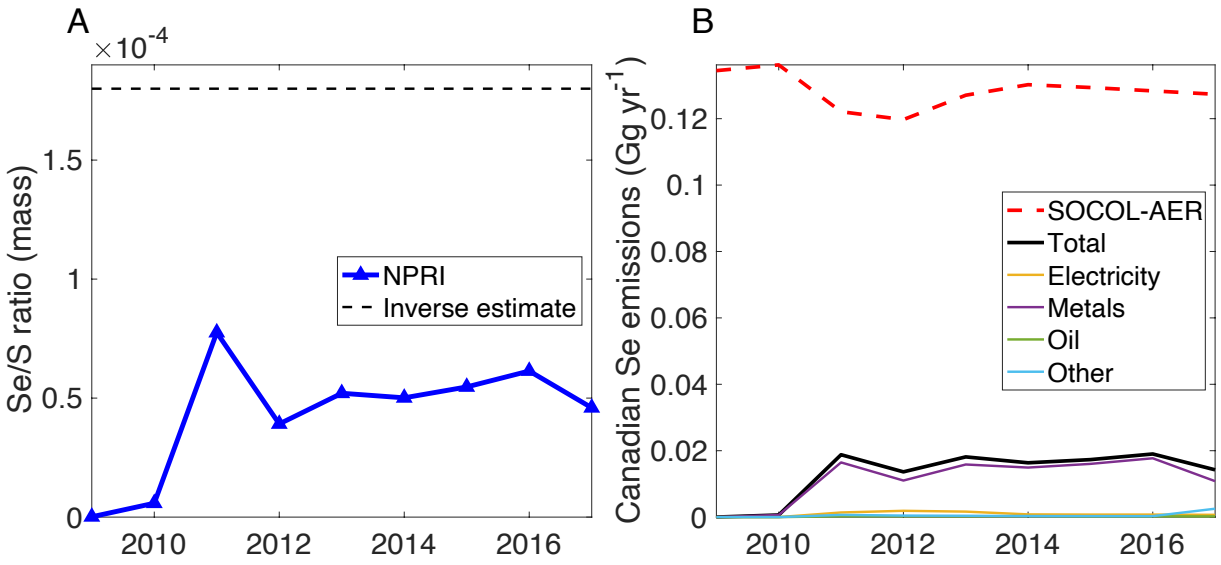

Supplementary Figure 12. Comparison of SOCOL-AER with emissions from the Canadian NPRI inventory. (a) The mean Se-to-S emission ratio for sources that report both S and Se emissions to the NPRI is shown in blue, which is compared to the inverse estimate of the Se-to-S emission ratio from Feinberg et al.[14]. **(b)** Total Canadian Se emissions are shown for SOCOL-AER (red dashed line) and the NPRI (black solid line). Colored solid lines show the Se emissions from different source categories in the NPRI.

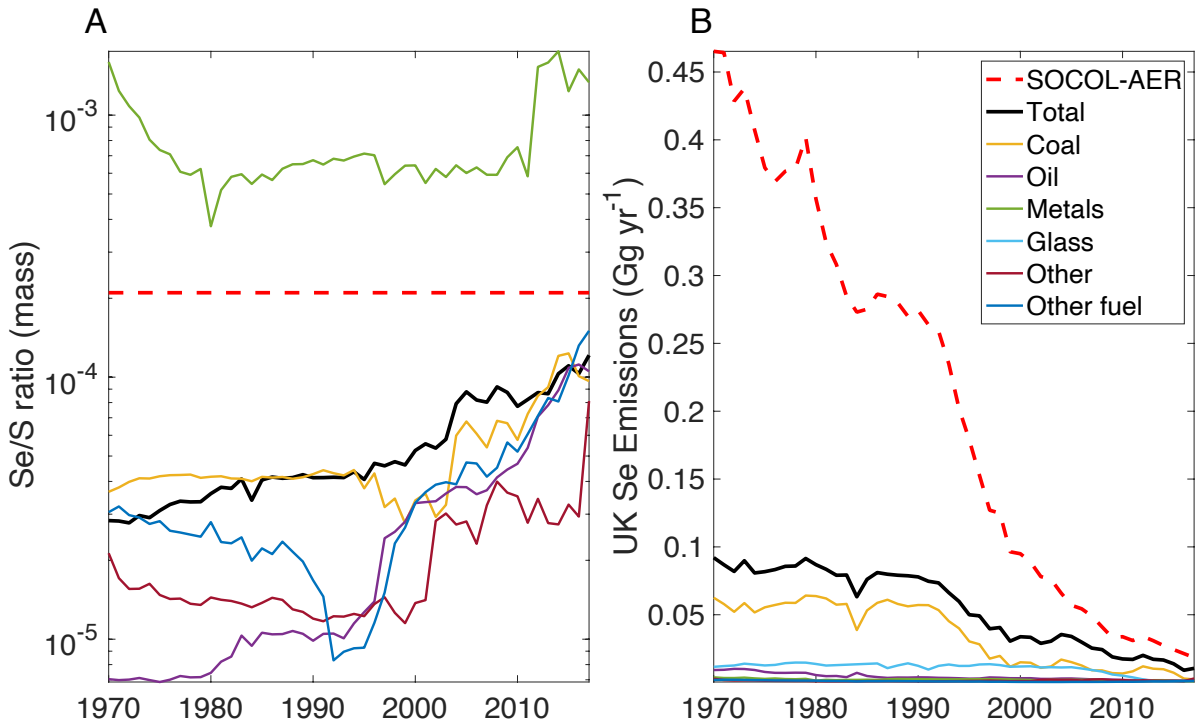

Supplementary Figure 13. Comparison of SOCOL-AER with emissions from the UK NAEI inventory. (a) Trends in Se-to-S emission ratios for different source categories in the NAEI are shown as solid lines. The overall Se-to-S emission ratio (black line) from the NAEI can be compared to the inverse estimate of the Se-to-S emission ratio for Europe from Feinberg et al.[14] (red dashed line). **(b)** Total UK Se emissions are shown for SOCOL-AER (red dashed line) and the NAEI (black solid line). Colored solid lines show the Se emissions from different source categories in the NAEI.

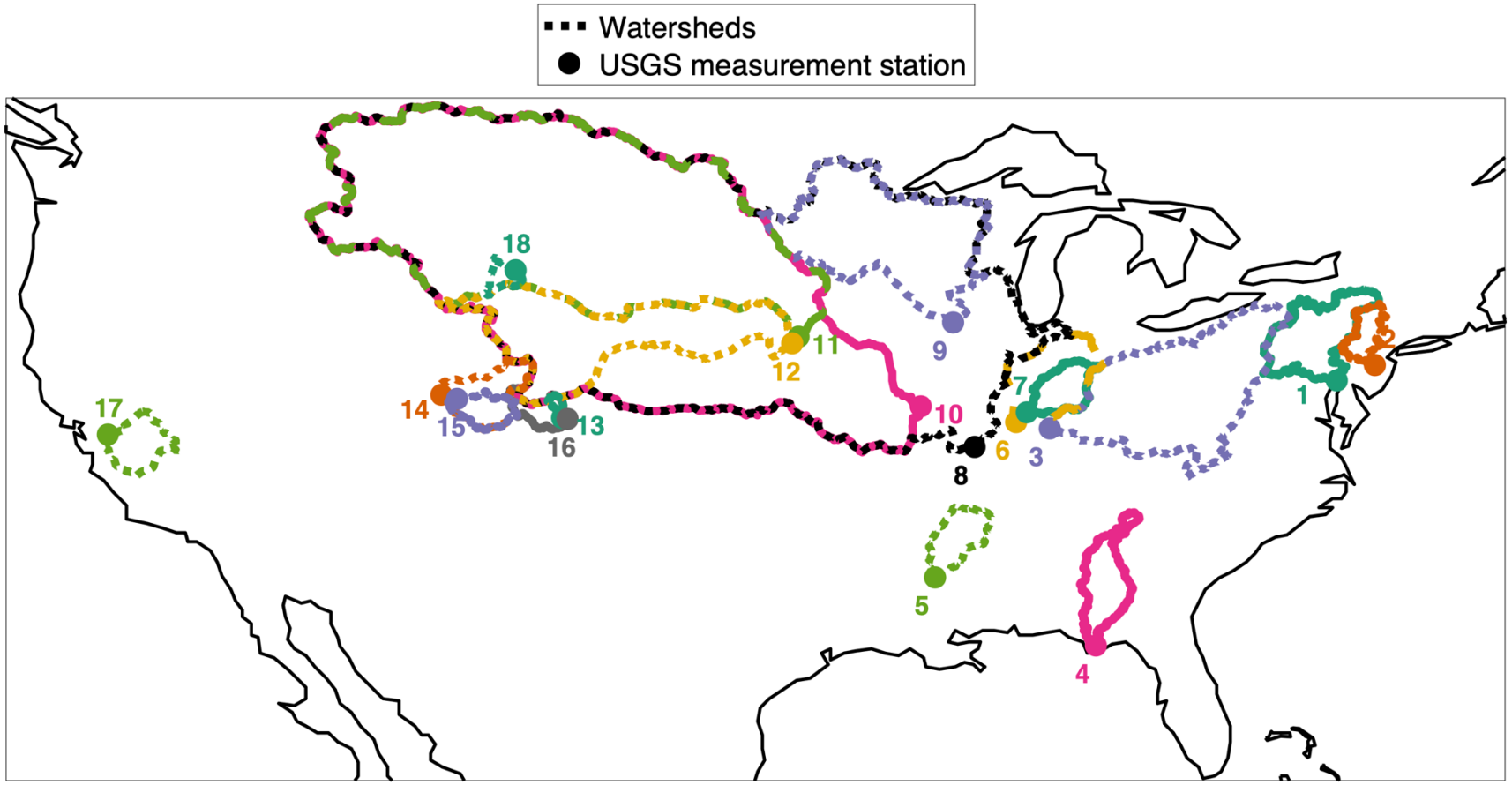

Supplementary Figure 14. Map of watersheds used in the study. The numbering of sites refers to Supplementary Table 4. The color and line style of the watershed boundaries are varied only to distinguish between neighboring or overlapping basins.

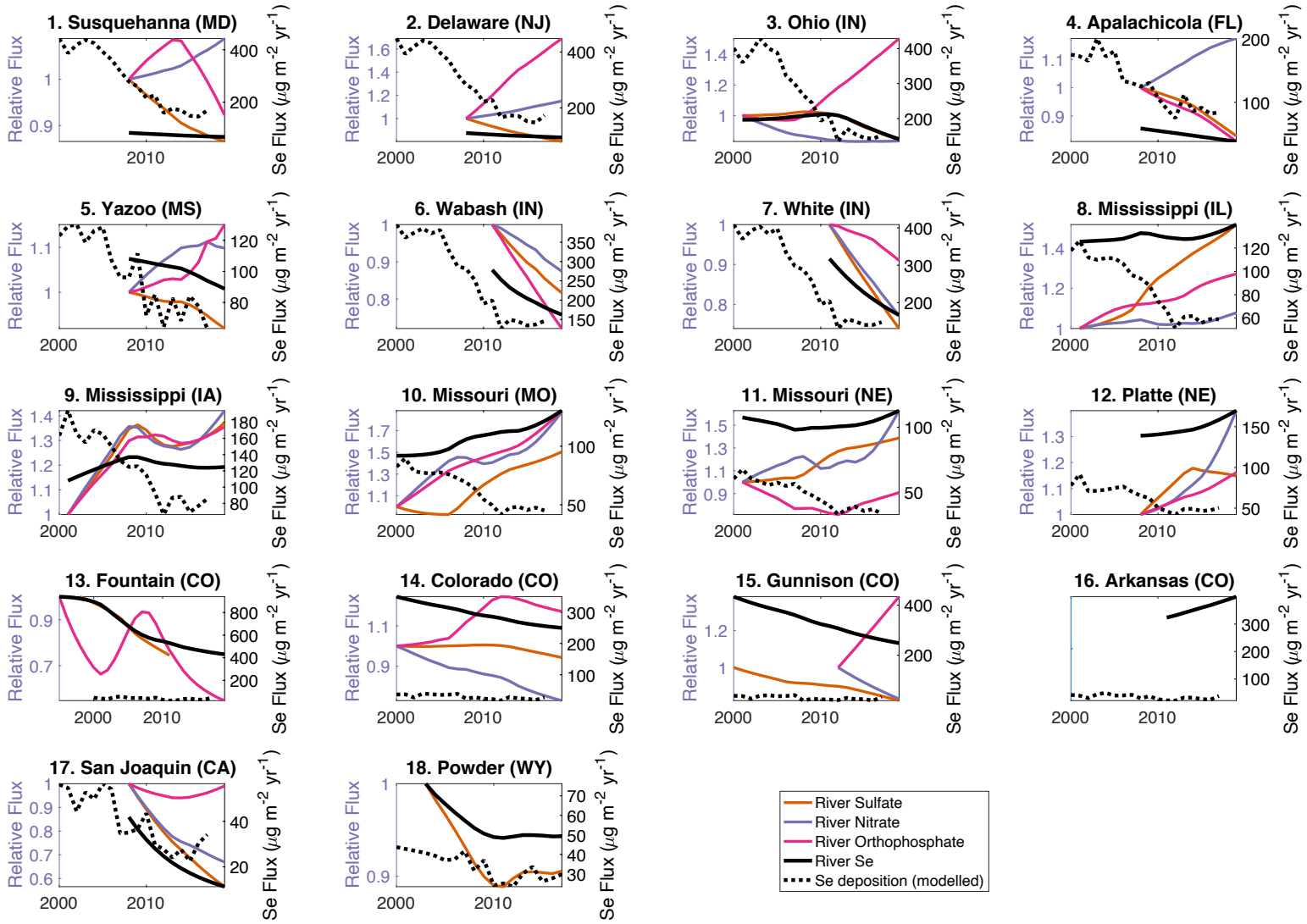

Supplementary Figure 15. Stream flux trends in USGS watersheds. Relative flux trends are shown for dissolved sulfate, nitrate and orthophosphate, based on flow-normalized WRTDS models. The modelled Se deposition flux and the flow-normalized dissolved Se flux are shown as absolute fluxes on the right axis. Modelled Se deposition is averaged over the area of each watershed, so that it can be directly compared with the stream Se flux.

1) Susquehanna River, MD (01578310)

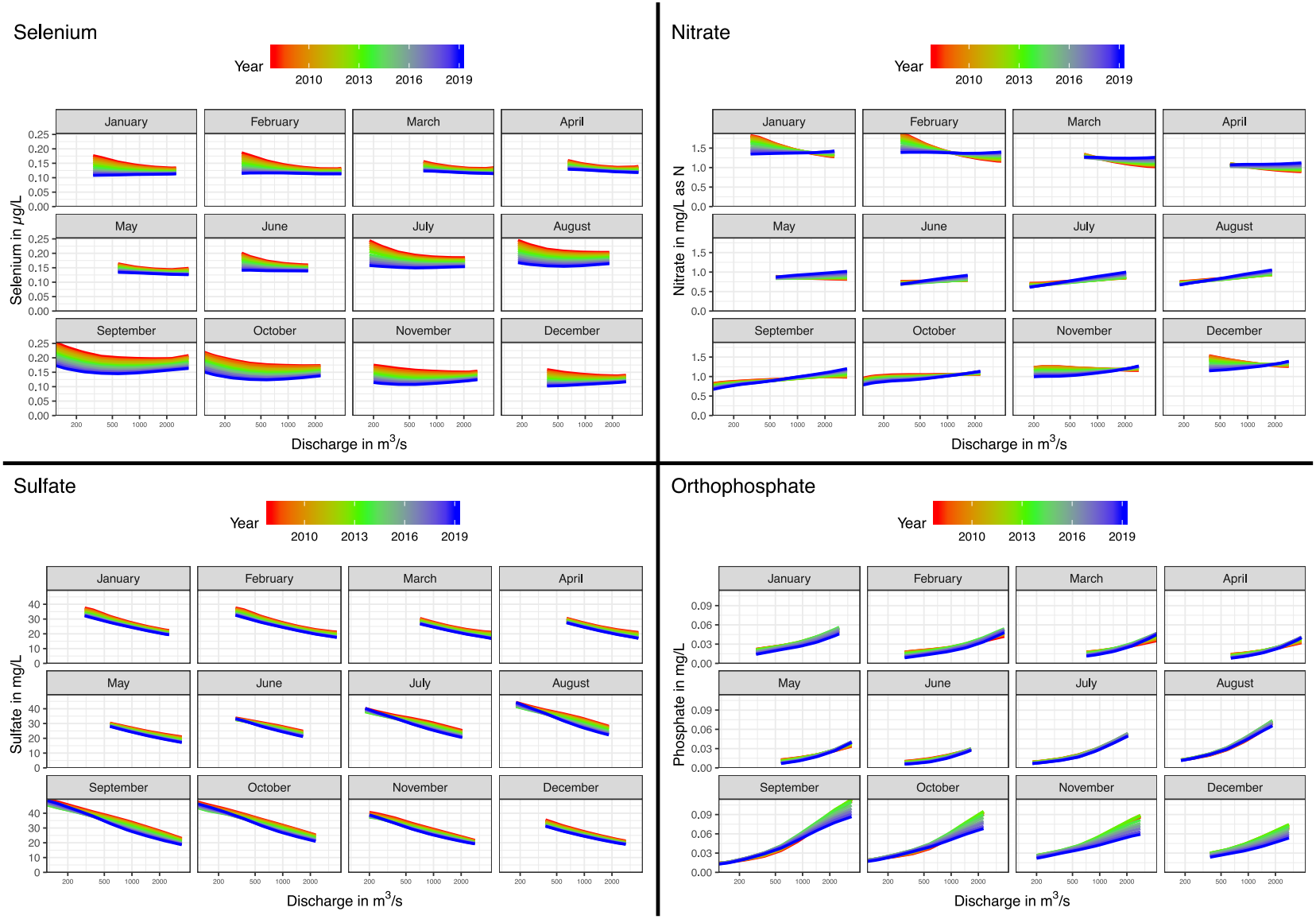

Supplementary Figure 16. Monthly concentration-discharge relationships for the Susquehanna River Basin.

2) Delaware River, NJ (01463500)

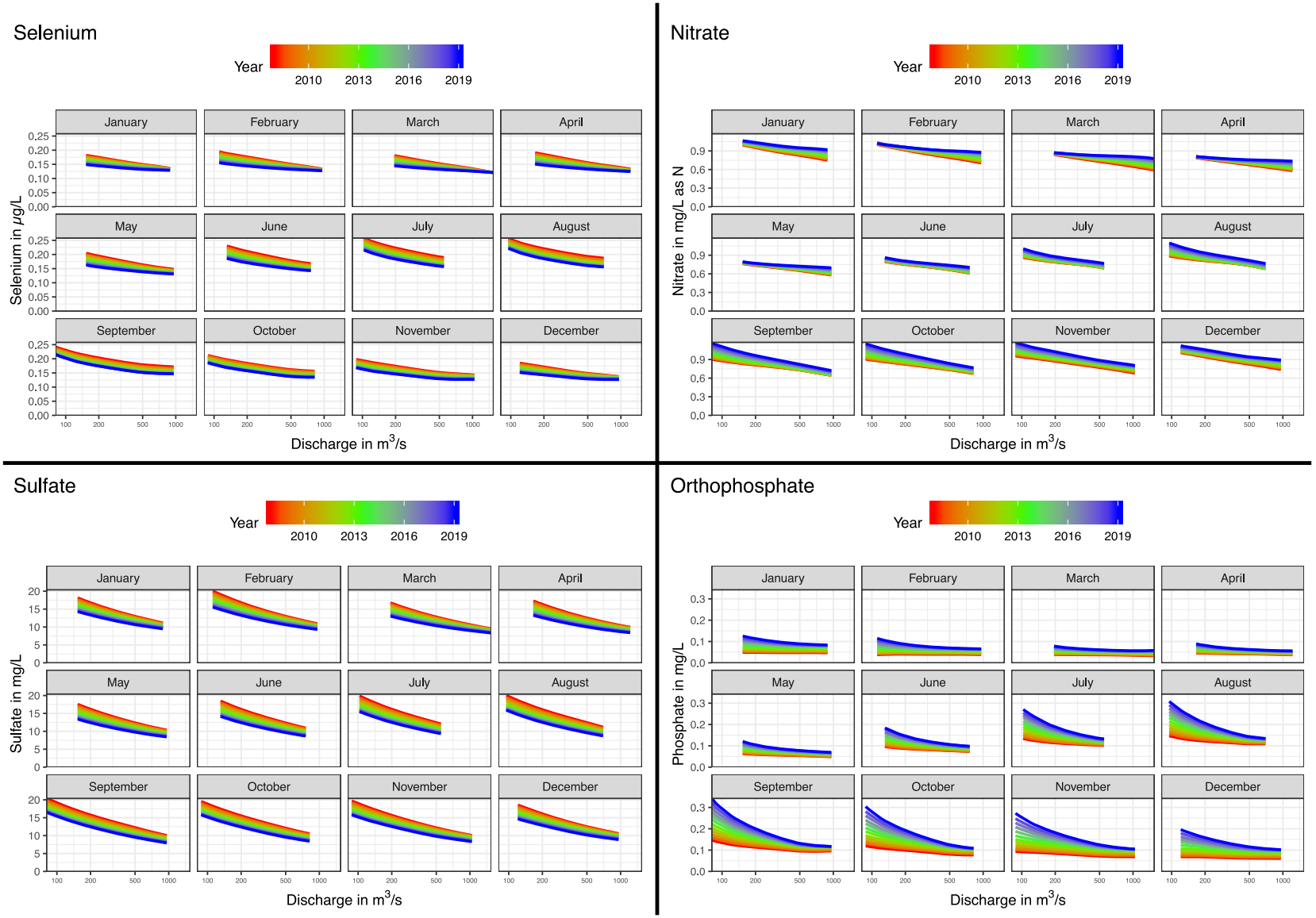

Supplementary Figure 17. Monthly concentration-discharge relationships for the Delaware River Basin.

3) Ohio River, IN (03303280)

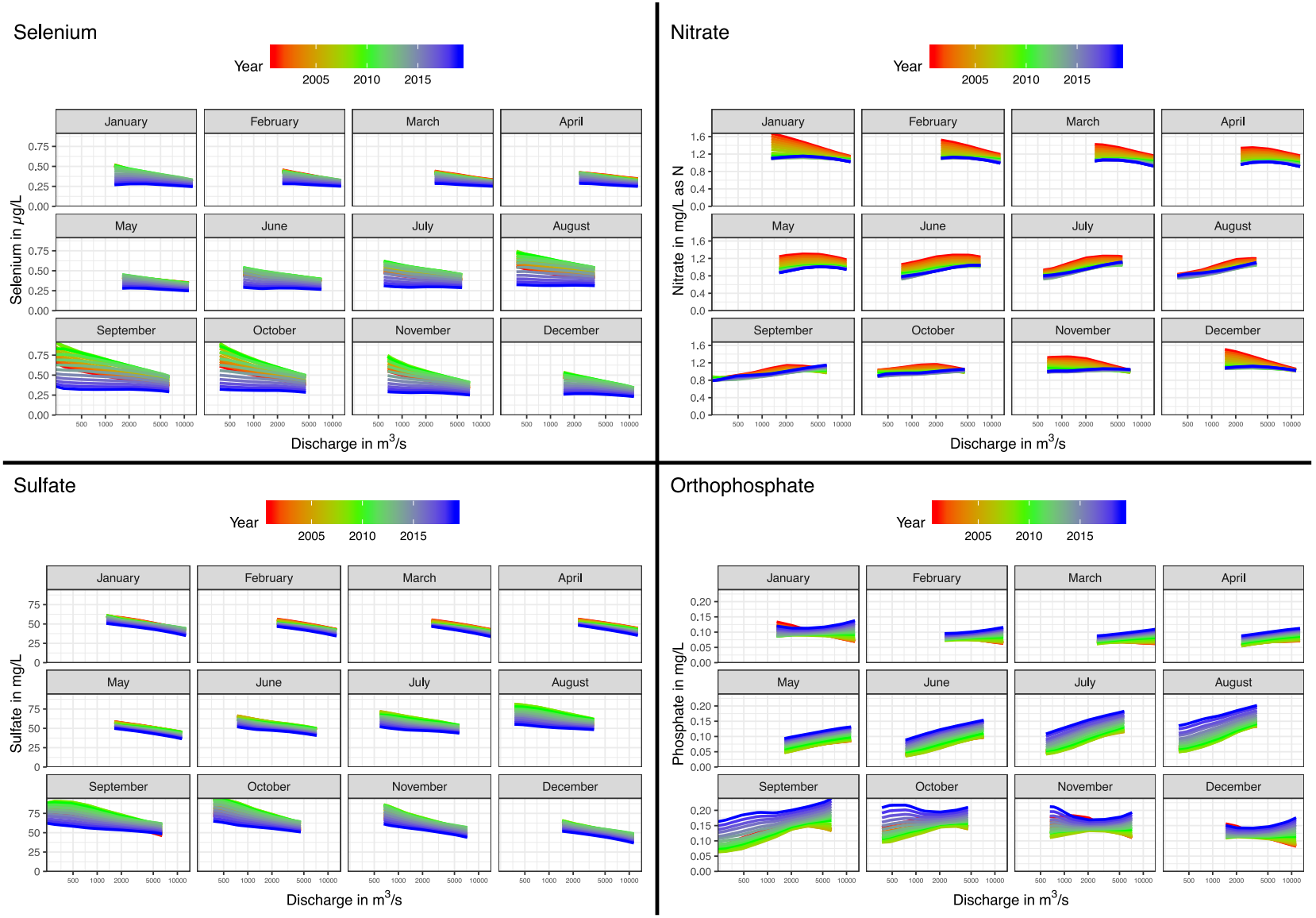

Supplementary Figure 18. Monthly concentration-discharge relationships for the Ohio River Basin.

8) Mississippi River, IL (07022000)

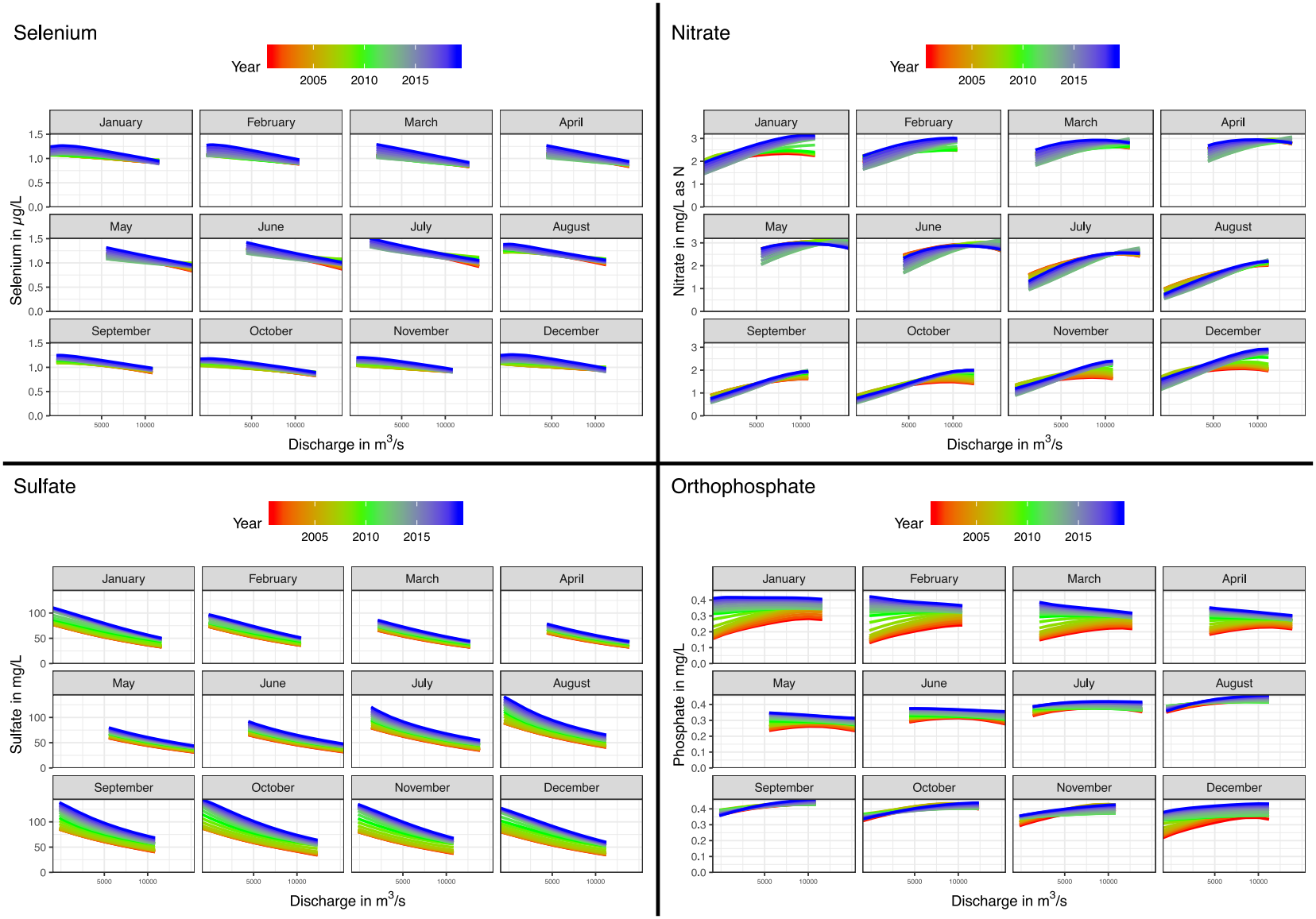

Supplementary Figure 19. Monthly concentration-discharge relationships for the Mississippi River Basin.

12) Platte River, NE (06805500)

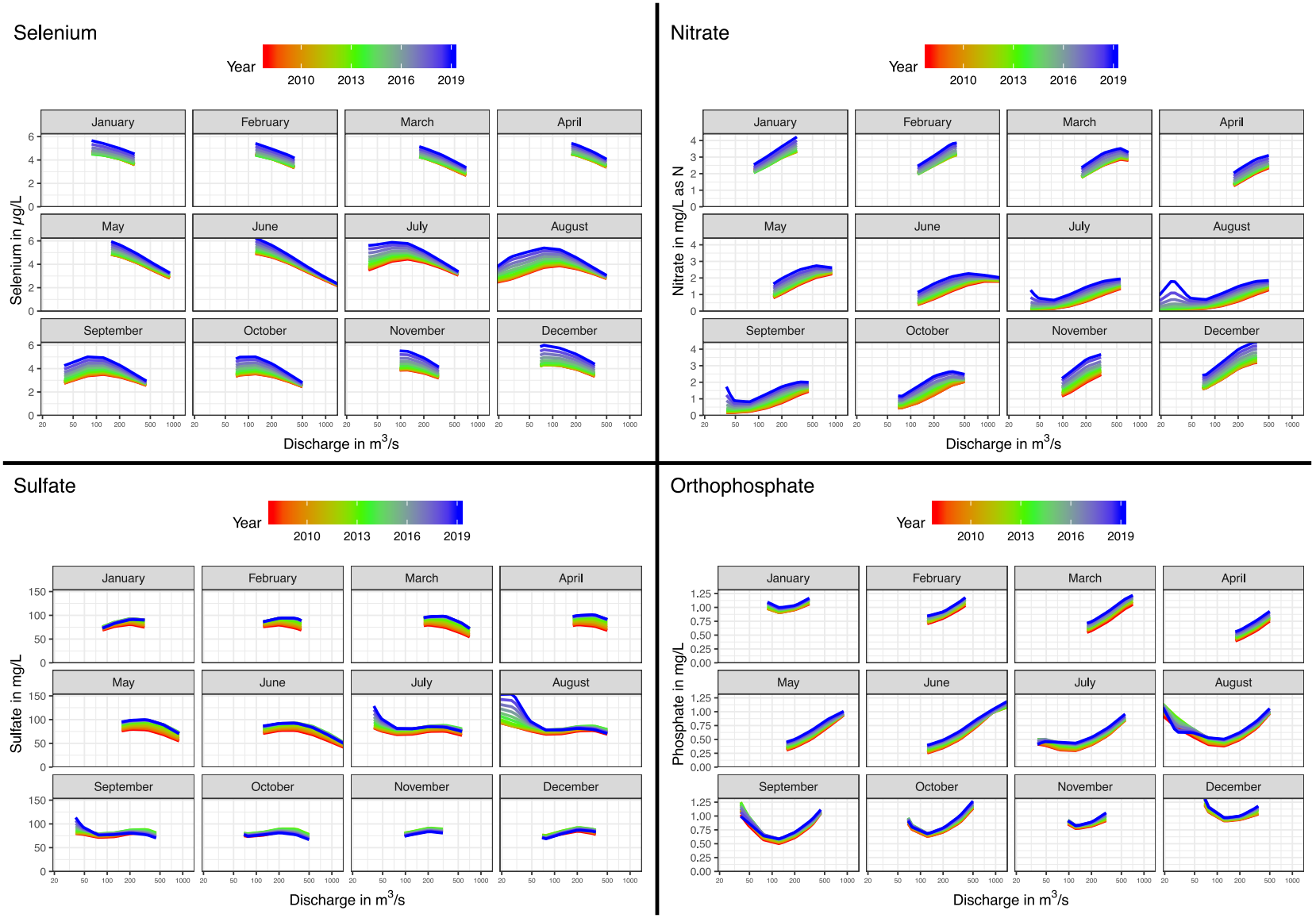

Supplementary Figure 20. Monthly concentration-discharge relationships for the Platte River Basin.

17) San Joaquin River, CA (11303500)

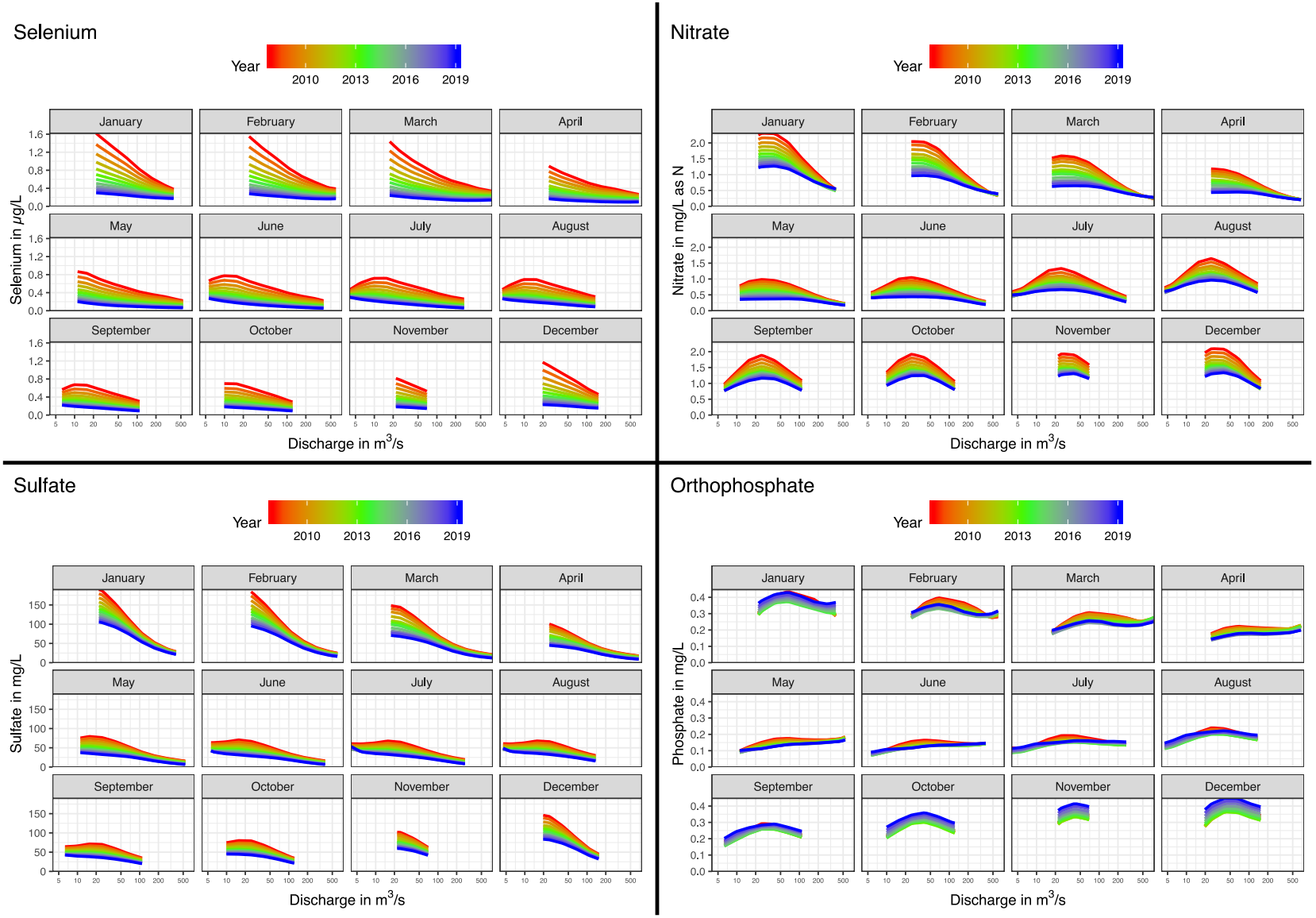

Supplementary Figure 21. Monthly concentration-discharge relationships for the San Joaquin River Basin.

Supplementary Table 1. Emissions of S and Se from different source categories (anthropogenic activities, volcanoes, marine biosphere, and terrestrial biosphere). Global fluxes are calculated from SOCOL-AER simulations for different time periods and socioeconomic projections for the future. Percentages in brackets below the flux values refer to the fraction of total emissions.

Source	Sulfur (Tg S yr^{-1})				Selenium (Gg Se yr^{-1})			
	1981–1985	2005–2009	2095–2099 SSP1–2.6	2095–2099 SSP5–8.5	1981–1985	2005–2009	2095–2099 SSP1–2.6	2095–2099 SSP5–8.5
Anthropogenic	65.2 (62%)	61.4 (60%)	4.2 (9%)	16.4 (28%)	12.4 (35%)	11.7 (34%)	0.8 (3%)	3.1 (12%)
Volcanic	12.6 (12%)	12.6 (12%)	12.6 (28%)	12.6 (22%)	3.8 (11%)	3.8 (11%)	3.8 (16%)	3.8 (14%)
Marine	27.8 (26%)	27.8 (27%)	28.3 (63%)	29.1 (50%)	14.2 (40%)	14.2 (41%)	14.4 (60%)	14.8 (55%)
Terrestrial	-	-	-	-	5.0 (14%)	5.0 (14%)	5.0 (21%)	5.0 (19%)
Total	**105.6**	**101.8**	**45.0**	**58.1**	**35.4**	**34.7**	**24.0**	**26.7**

Supplementary Table 2. Sulfur deposition to agricultural areas for different continents and simulations in units of mg S m^{-2} yr^{-1}. Mean values are listed, with 10th and 90th percentile values (due to spatial variability) given in parentheses. Agricultural model grid cells are defined where the fraction of cropland or pasture represents more than 25% of the land area in the Ramankutty et al.[40] dataset.

Continents	1981–1985	2005–2009	2095–2099 SSP1–2.6	2095–2099 SSP5–8.5	2095–2099 SSP5–8.5 (2005–2009 climate)
Asia	537.9 (143.2–1221.1)	1045.5 (187.3–2609.4)	86.7 (18.0–169.0)	206.0 (34.3–452.7)	211.2 (38.3–443.6)
Europe	2126.2 (556.5–4441.4)	637.8 (281.4–1200.5)	89.2 (32.4–146.1)	199.7 (64.9–406.3)	216.7 (65.1–465.3)
North America	718.6 (180.3–1840.8)	404.5 (83.9–960.4)	49.4 (13.4–84.4)	115.0 (30.8–252.2)	118.0 (27.4–246.6)
Africa	169.8 (46.2–266.0)	183.3 (64.6–304.1)	98.4 (21.9–188.9)	141.5 (31.7–283.2)	143.7 (35.3–273.9)
Australia	91.8 (44.9–165.7)	91.1 (42.5–172.6)	53.6 (28.9–85.3)	59.6 (27.6–97.0)	58.2 (27.8–96.6)
South America	266.4 (73.1–364.9)	276.5 (61.7–355.3)	156.9 (46.4–165.3)	214.3 (60.6–331.7)	235.8 (63.4–326.8)

Supplementary Table 3. Selenium deposition to agricultural areas for different continents and simulations in units of µg Se m^{-2} yr^{-1}. Mean values are listed, with 10th and 90th percentile values (due to spatial variability) given in parentheses. Agricultural model grid cells are defined where the fraction of cropland or pasture represents more than 25% of the land area in the Ramankutty et al.[40] dataset.

Continents	1981–1985	2005–2009	2095–2099 SSP1–2.6	2095–2099 SSP5–8.5	2095–2099 SSP5–8.5 (2005–2009 climate)
Asia	130.6 (37.3–269.7)	225.6 (39.7–526.2)	43.7 (7.9–90.7)	65.4 (11.1–139.5)	66.1 (12.8–131.7)
Europe	429.7 (109.0–920.8)	140.7 (63.5–249.6)	35.5 (15.1–51.2)	54.7 (21.7–94.3)	60.5 (22.7–111.2)
North America	155.8 (36.8–390.1)	97.4 (21.4–225.5)	29.4 (6.6–50.6)	41.3 (11.4–87.0)	42.7 (9.0–80.5)
Africa	67.5 (16.1–108.0)	70.7 (20.4–114.7)	52.8 (9.4–93.7)	63.0 (13.9–107.0)	63.7 (15.9–110.8)
Australia	38.0 (21.8–60.2)	37.4 (20.5–58.8)	34.9 (18.9–48.7)	32.5 (17.1–51.8)	31.6 (17.7–51.0)
South America	123.3 (31.2–177.5)	125.6 (25.2–171.8)	99.2 (21.5–132.9)	112.2 (24.3–176.6)	115.1 (25.8–164.6)

Supplementary Table 4. USGS stream gauge stations used in this study.

#	Watershed name	State	Site ID	Latitude (° N)	Longitude (° W)	Years analyzed	# Se samples
1	Susquehanna River	MD	01578310	39.66	76.17	2008–2019	163
2	Delaware River	NJ	01463500	40.22	74.78	2008–2019	164
3	Ohio River	IN	03303280	37.90	86.71	2001–2019	254
4	Apalachicola River	FL	02359170	29.95	85.02	2008–2019	148
5	Yazoo River	MS	07288955	32.44	90.91	2008–2019	185
6	Wabash River	IN	03378500	38.13	87.94	2011–2019	118
7	White River	IN	03374100	38.49	87.55	2011–2019	148
8	Mississippi River	IL	07022000	37.22	89.46	2001–2019	260
9	Mississippi River	IA	05420500	41.78	90.25	2001–2019	245
10	Missouri River	MO	06934500	38.71	91.44	2000–2019	276
11	Missouri River	NE	06610000	41.26	95.92	2001–2019	261
12	Platte River	NE	06805500	41.02	96.16	2008–2019	158
13	Fountain Creek	CO	07106500	38.29	104.60	1995–2019	230
14	Colorado River	CO	09163500	39.13	109.03	2000–2019	236
15	Gunnison River	CO	09152500	38.98	108.45	2000–2019	169
16	Arkansas River	CO	07109500	38.25	104.40	2011–2019	118
17	San Joaquin River	CA	11303500	37.67	121.27	2008–2019	183
18	Powder River	WY	06313500	43.70	106.31	2003–2017	251

Supplementary References

1. Collins, M. *et al.* Long-term climate change: projections, commitments and irreversibility. in *Climate Change 2013: The Physical Science Basis* (eds. Stocker, T. F. et al.) 1029–1136 (IPCC AR5, Cambridge University Press, 2013).
2. Carslaw, K. S. *et al.* A review of natural aerosol interactions and feedbacks within the Earth system. *Atmos. Chem. Phys.* **10**, 1701–1737 (2010).
3. Cameron-Smith, P., Elliott, S., Maltrud, M., Erickson, D. & Wingenter, O. Changes in dimethyl sulfide oceanic distribution due to climate change. *Geophys. Res. Lett.* **38**, 1–5 (2011).
4. Mahmood, R., von Salzen, K., Norman, A.-L., Galí, M. & Levasseur, M. Sensitivity of Arctic sulfate aerosol and clouds to changes in future surface seawater dimethylsulfide concentrations. *Atmos. Chem. Phys.* **19**, 6419–6435 (2019).
5. Galí, M., Devred, E., Babin, M. & Levasseur, M. Decadal increase in Arctic dimethylsulfide emission. *Proc. Natl. Acad. Sci.* **116**, 19311–19317 (2019).
6. Vogt, M. *et al.* Dynamics of dimethylsulphoniopropionate and dimethylsulphide under different CO2 concentrations during a mesocosm experiment. *Biogeosciences* **5**, 407–419 (2008).
7. Six, K. D. *et al.* Global warming amplified by reduced sulphur fluxes as a result of ocean acidification. *Nat. Clim. Chang.* **3**, 975–978 (2013).
8. Halloran, P. R., Bell, T. G. & Totterdell, I. J. Can we trust empirical marine DMS parameterisations within projections of future climate? *Biogeosciences* **7**, 1645–1656 (2010).
9. Boucher, O. *et al.* Clouds and Aerosols. in *Climate Change 2013: The Physical Science Basis* (eds. Stocker, T. F. et al.) 571–658 (IPCC AR5, Cambridge University Press, 2013).
10. Lin, G., Penner, J. E. & Zhou, C. How will SOA change in the future? *Geophys. Res. Lett.* **43**, 1718–1726 (2016).
11. Neal, C., Kirchner, J. & Reynolds, B. Plynlimon research catchment hydrochemistry. (2013). doi:10.5285/44095e17-43b0-45d4-a781-aab4f72da025
12. Norris, D. A. *et al.* Plynlimon research catchment hydrochemistry (2011-2016). (2017). doi:10.5285/794c609b-da62-4a42-a4c1-267219865bb1
13. Gidden, M. J. *et al.* Global emissions pathways under different socioeconomic scenarios for use in CMIP6: A dataset of harmonized emissions trajectories through the end of the century. *Geosci. Model Dev.* **12**, 1443–1475 (2019).
14. Feinberg, A., Stenke, A., Peter, T. & Winkel, L. H. E. Constraining Atmospheric Selenium Emissions Using Observations, Global Modeling, and Bayesian Inference. *Environ. Sci. Technol.* **54**, 7146–7155 (2020).
15. Tian, H. Z. *et al.* Quantitative assessment of atmospheric emissions of toxic heavy metals from anthropogenic sources in China: historical trend, spatial distribution, uncertainties, and control policies. *Atmos. Chem. Phys.* **15**, 10127–10147 (2015).
16. Langner, B. E. Selenium and Selenium Compounds. *Ullmann's Encyclopedia of Industrial Chemistry* (2000). doi:10.1002/14356007.a23_525
17. Passant, N. R. Estimation of Estimation of Uncertainties in the National Atmospheric Emissions Inventory. 96–97 (2003). Available at: https://uk-air.defra.gov.uk/assets/documents/reports/cat07/AEAT1039_finaldraft_v2.pdf.
18. Richmond, B. *et al.* UK Informative Inventory Report (1990 to 2018). 6287–6308 (2020). Available at: https://uk-

air.defra.gov.uk/assets/documents/reports/cat07/2003131327_GB_IIR_2020_v1.0.pdf.
19. Rice, K. C., Scanlon, T. M., Lynch, J. A. & Cosby, B. J. Decreased Atmospheric Sulfur Deposition across the Southeastern U.S.: When Will Watersheds Release Stored Sulfate? *Environ. Sci. Technol.* **48**, 10071–10078 (2014).
20. David, M. B., Gentry, L. E. & Mitchell, C. A. Riverine Response of Sulfate to Declining Atmospheric Sulfur Deposition in Agricultural Watersheds. *J. Environ. Qual.* **45**, 1313–1319 (2016).
21. Siemion, J., McHale, M. R., Lawrence, G. B., Burns, D. A. & Antidormi, M. Long-term Changes in Soil and Stream Chemistry across an Acid Deposition Gradient in the Northeastern United States. *J. Environ. Qual.* **47**, 410–418 (2018).
22. Hinckley, E.-L. S., Crawford, J. T., Fakhraei, H. & Driscoll, C. T. A shift in sulfur-cycle manipulation from atmospheric emissions to agricultural additions. *Nat. Geosci.* **13**, 597–604 (2020).
23. Smith, V. H. Eutrophication of freshwater and coastal marine ecosystems a global problem. *Environ. Sci. Pollut. Res.* **10**, 126–139 (2003).
24. Plant, J. A. *et al.* Arsenic and Selenium. in *Treatise on Geochemistry: Second Edition* 13–57 (Elsevier, Oxford, UK, 2014).
25. Stephens, D. W., Waddell, B., Peltz, L. A. & Miller, J. B. *Detailed Study of Selenium and Selected Elements in Water, Bottom Sediment, and Biota Associated with Irrigation Drainage in the Middle Green River Basin Utah, 1988-90*. (1992). doi:10.3133/wri924084
26. Seiler, R. L. & Skorupa, J. P. Identification of areas at risk for selenium contamination in the western United States. in *Water Resources at Risk* LL85–LL94 (American Institute of Hydrology, Minneapolis, Minnesota, 1995).
27. Engberg, R. A. Selenium Budgets for Lake Powell and the Upper Colorado River Basin. *JAWRA J. Am. Water Resour. Assoc.* **35**, 771–786 (1999).
28. Hamilton, S. J. Hypothesis of Historical Effects From Selenium on Endangered Fish in the Colorado River Basin. *Hum. Ecol. Risk Assess. An Int. J.* **5**, 1153–1180 (1999).
29. Quinn, N. W. T. Policy Innovation and Governance for Irrigation Sustainability in the Arid, Saline San Joaquin River Basin. *Sustainability* **12**, 4733 (2020).
30. Winkel, L. H. E. *et al.* Environmental selenium research: From microscopic processes to global understanding. *Environ. Sci. Technol.* **46**, 571–579 (2012).
31. Singh, A., Quinn, N. W. T., Benes, S. E. & Cassel, F. Policy-Driven Sustainable Saline Drainage Disposal and Forage Production in the Western San Joaquin Valley of California. *Sustainability* **12**, 6362 (2020).
32. Heidel, K., Roy, S., Creager, C., Chung, C. & Grieb, T. Conceptual Model for Nutrients in the Central Valley and Sacramento-San Joaquin Delta. (2006). Available at: https://www.waterboards.ca.gov/centralvalley/water_issues/drinking_water_policy/final_nutrient_report_lowres.pdf.
33. Hirsch, R. M. & De Cicco, L. A. User guide to Exploration and Graphics for RivEr Trends (EGRET) and dataRetrieval: R packages for hydrologic data. (2015). doi:10.3133/tm4A10
34. Naftz, D. L. & Rice, J. A. Geochemical processes controlling selenium in ground water after mining, Powder River Basin, Wyoming, U.S.A. *Appl. Geochemistry* **4**, 565–575 (1989).
35. Dreher, G. B. & Finkelman, R. B. Selenium mobilization in a surface coal mine, Powder River Basin, Wyoming, U.S.A. *Environ. Geol. Water Sci.* **19**, 155–167 (1992).
36. Feaster, S. & Cates, K. Powder River Basin Coal Industry Is in Long-Term Decline.

(2019). Available at: https://ieefa.org/wp-content/uploads/2019/03/Powder-River-Basin-Coal-Industry-Is-in-Long-Term-Decline_March-2019.pdf.
37. Godsey, S. E., Kirchner, J. W. & Clow, D. W. Concentration--discharge relationships reflect chemostatic characteristics of US catchments. *Hydrol. Process. An Int. J.* **23**, 1844–1864 (2009).
38. Basu, N. B., Thompson, S. E. & Rao, P. S. C. Hydrologic and biogeochemical functioning of intensively managed catchments: A synthesis of top-down analyses. *Water Resour. Res.* **47**, W00J15 (2011).
39. Moatar, F., Abbott, B. W., Minaudo, C., Curie, F. & Pinay, G. Elemental properties, hydrology, and biology interact to shape concentration-discharge curves for carbon, nutrients, sediment, and major ions. *Water Resour. Res.* **53**, 1270–1287 (2017).
40. Ramankutty, N., Evan, A. T., Monfreda, C. & Foley, J. A. Farming the planet: 1. Geographic distribution of global agricultural lands in the year 2000. *Global Biogeochem. Cycles* **22**, GB1003 (2008).